Cretaceous Research 35 (2012) 94–117

Contents lists available at SciVerse ScienceDirect

Cretaceous Research

journal homepage: www.elsevier.com/locate/CretRes

The geology and palaeoecology of the newly discovered Cretaceous neosauropod hydrothermal nesting site in Sanagasta (Los Llanos Formation), La Rioja, northwest Argentina

Lucas E. Fiorelli [a,*], Gerald Grellet-Tinner [a,b,c], Pablo H. Alasino [a,d], Eloisa Argañaraz [e]

[a] Centro Regional de Investigaciones Científicas y Transferencia Tecnológica (CRILAR), Entre Ríos y Mendoza s/n, (5301) Anillaco, La Rioja, Argentina
[b] Field Museum, Chicago, USA
[c] The Journey Museum, Rapid City, USA
[d] Universidad Nacional de La Rioja, Av. Dr. Rene Favaloro (5300), La Rioja, Argentina
[e] CIPAL, Av. Vélez Sarsfield 299, (5000) Córdoba, Argentina

ARTICLE INFO

Article history:
Received 8 September 2011
Accepted in revised form 2 December 2011
Available online 13 December 2011

Keywords:
Geology
Sedimentology
Hydrothermal palaeoenvironment
Cretaceous
Sanagasta
Neosauropod
Nesting site
La Rioja

ABSTRACT

The recent discovery of the Cretaceous Sanagasta geothermal nesting site in the Los Llanos Formation, La Rioja Province, northwestern Argentina, has shed light on new and unexpected neosauropod reproductive behaviours. Here we recapitulate the palaeontological discovery at Sanagasta and the oological characterization of the nesting site (reported in 2010). In addition, we describe in detail the geology, sedimentology, petrology, and geochemistry of the nesting site with the goals of assessing the palaeoenvironment of the Los Llanos Formation at this site. The Sanagasta Geologic Park, where the nesting site is located, represents a local expression of a geothermal process that occured in the Sierras Pampeanas during the Cretaceous Period. This geothermal cycle allows for the first time an Early Cretaceous dating (Hauterivian–Aptian) for the Los Llanos Formation, which is further supported by the occurrence of notosuchians, and ornithopod, sauropod and theropod dinosaurs in other exposures of the same formation in La Rioja Province. As such, in addition to shedding light on neosauropod palaeobiology and their nesting environment, this investigation clarifies longstanding geological issues pertaining to the sedimentary basins in the Sierras Pampeanas Orientales (central-west Argentina).

1. Introduction

The southwest region of La Rioja Province, northwest Argentina, already well-known for its continental Triassic Los Chañares and Los Colorados formations (Bonaparte, 1978, 1997; Rogers et al., 2001; Arcucci et al., 2004), has yielded avian-like footprints from the Late Triassic–Early Jurassic Santo Domingo Formation (Melchor et al., 2002), and fragmentary fossils identified as belonging to titanosaur dinosaurs in the Precordillera Cretaceous beds (Arcucci et al., 2005). Although Ciccioli et al. (2005) and Tedesco et al. (2007) reported the discovery of a thick Early Cretaceous red-bed complex, the Ciénaga del Río Huaco Formation, in the Precordillera Central (La Rioja and San Juan provinces), the Mesozoic sedimentary basins of the Sierras Pampeanas in central-west Argentina were poorly known because of limited study and understanding of the regional geology.

The Los Llanos Formation (Bordas, 1941; Zuzek, 1978; see also Limarino and Poma, 1999 and Ezpeleta et al., 2006) in the Sierras Pampeanas of the central region of the La Rioja Province, crops out as a heterogeneous fluvio-eolian unit with abundant calcretes and palaeosols. This succession of up to about 40 m is also substantially exposed in the Sierra Brava, Sierra de Ulapes-Las Minas, and Sierra de Los Llanos (type locality of this formation in exposures on the western slope of this mountain range). Historically, Bodenbender (1911) named the "Estratos de Los Llanos" for this series of sedimentary units scattered in La Rioja Province and dated these outcrops as Late Cretaceous. However, the "Estratos de Los Llanos" were later included in the Los Llanos Formation by Bordas (1941) and Zuzek (1978). In addition, Bodenbender's work was revised between 1930 and the 1960s and correlations with Paleogene and Neogene outcrops from other neighbouring provinces (Rusconi, 1936; Bordas, 1941; Pascual, 1954; Guiñazú, 1962) constrained the age of the exposures located to the south of La Rioja Province to the Cenozoic, a dating that prevailed until recently (Limarino and Poma, 1999; Ezpeleta et al., 2006; Ruskin,

* Corresponding author.
E-mail address: lfiorelli@crilar-conicet.gob.ar (L.E. Fiorelli).

0195-6671/$ – see front matter © 2011 Elsevier Ltd. All rights reserved.
doi:10.1016/j.cretres.2011.12.002

2006; Dávila et al., 2007; Ruskin et al., 2011). Although the Los Llanos Formation occurs extensively throughout the province, its exposures are relatively limited on the eastern side of the Sierra de Velasco (part of Sierras Pampeanas) and mostly located within the Sanagasta Valley in the central region of this mountain range (Fig. 1A). Interestingly, fragmentary dinosaur eggshells in the outcrops of the Sanagasta Valley were reported in 2007 (Tauber, 2007) and led to the reversion of the age of this locality to Bodenbender's Cretaceous dating. Considering the former information, in 2007 the CRILAR (see section on abbreviations) Geoscience Department launched a series of palaeontological field trips to Sanagasta Geologic Park (SGP) (Fig. 1), where dinosaur eggshells were apparently found (see Tauber, 2007). These first field trips resulted in the discovery of an impressive dinosaur nesting site at Sanagasta, perhaps the most palaeobiologically significant South American nesting site outside Patagonia (Grellet-Tinner and Fiorelli, 2010). This neosauropod nesting site has yielded numerous egg clutches with several complete eggs. To date, more than 70 clutches, with up to 35 complete eggs in some, have been discovered within 300,000 m^2 (Fig. 1C). This stunning discovery of Cretaceous colonial nesting presents several intriguing aspects of dinosaur reproduction behaviour and a surprising symbiotic/commensalism relationship from a Margulisian point of view (Margulis, 1998) between sauropod nesting behaviours and a geothermal palaeoenvironment (Grellet-Tinner and Fiorelli, 2010). This site is unique as it is the first to offer an answer to the question of what possible ecological settings triggered the Sanagasta neosauropods repeatedly to choose this location to lay their eggs, a subject that had never clearly been addressed before for other sauropod nesting sites (Grellet-Tinner and Fiorelli, 2010).

The goals of this paper are to complement the previous report by Grellet-Tinner and Fiorelli (2010) by presenting a complete and comprehensive geological description of the Sanagasta nesting site with ensuing sedimentological, petrographic, geochemical interpretations, and assessing the regional palaeoenvironment of the Los Llanos Formation at the site and in Sanagasta valley. As such, this work provides a precise geological background for neosauropod nesting behaviour and furthermore, helps understanding of the geological issues related to the sedimentary basins in the Sierras Pampeanas (central-west Argentina) and their dating.

Institutional abbreviations. CRILAR-Pv, Centro Regional de Investigaciones Científicas y Transferencia Tecnológica La Rioja, La Rioja province, Argentina; MACN, Museo Argentino de Ciencias Naturales "Bernardino Rivadavia", Buenos Aires, Argentina; SGP, Sanagasta Geologic Park; UNSL, Universidad Nacional de San Luís, San Luís Province, Argentina.

2. Material

2.1. Specimens for palaeontological analyses

The Sanagasta egg clutch, egg and eggshell specimens are curated at the provincial palaeontological repository (CRILAR). More specimens are still in-situ at the nesting site, which is now a protected and preserved fossil site. All the specimens for this study are in Table 1 with explanatory annotations.

2.2. Samples for petrographic analyses

Thirty-five rock samples from different SGP sectors and related outcrops in the Sanagasta Valley (Fig. 1; Table 1) were collected for petrographic and sedimentologic analyses and observations. The samples for petrographic thin section were taken from four sedimentary levels: upper level of the Sauces Formation (Lower Permian, nearly 5 m below the egg-bearing horizon); Lower Cretaceous level (3 m below the eggs); mid Cretaceous horizon (1.5 m below the eggs); and Upper Cretaceous horizon associated with the clutches and eggs (Fig. 2).

2.3. Fossil and petrographic samples for geochemical analyses

The eggshell specimens were collected from three different sites within the Sanagasta Valley (Table 1) and coded SAN-SSA-C10, -SSF-C11 and -SSE-C4 (see Fig. 1). Sedimentary samples were selected from three different levels at each site: the upper level of the Sauces Formation (Lower Permian); Lower Cretaceous horizon (3 m below the eggs); and Upper Cretaceous horizon with the clutches and eggs (see Fig. 2, SGP profile A). The specimens for geochemical analyses were coded SAN 1, 2, and 6 (Upper Permian, Lower Cretaceous and Upper Cretaceous levels at sub-site H, respectively); SAN 3, 4, and 5 (the same three levels at sub-site F, respectively); and SAN 7, 8, and (the same three levels at the Los Barquitos locality, respectively). The location of the each site is shown in Fig. 1.

3. Methods

Thin sections were made at the (CRILAR) Petrographic Laboratory. Observations were obtained under a stereoscopic microscope (Leica® MZ12) and Leica® DM LB light and petrographic® DM2500 P microscopes. The images were captured with a digital camera (Leica® DFC295) attached to the microscope and connected to a computer for processing, editing, and measurements. Although additional microcharacterizations will be undertaken in the future, a limited amount of SEM microcharacterization has already been carried out at the MACN microscope laboratory in Buenos Aires (http://www.macn.secyt.gov.ar/) and at the laboratory of the Universidad Nacional de San Luís (San Luís Province http://labmem.unsl.edu.ar/). SEM analyses were undertaken using a Philips® Scanning Electron Microscope XL 30 (at MACN) and a LEO® 1450VP Scanning Electron Microscope (at UNSL). Each specimen was coated with 60% gold and 40% palladium for 15 min (3 Armstrong/seg.) in a Thermo VG Scientific SC 7620. The SEM analyses were conducted at 10 kv and the scale bars were embedded in the images during their acquisition. The samples for thin section and SEM analysis are from complete eggs and isolated eggshell fragments with sediments from the main nesting site (see Grellet-Tinner and Fiorelli, 2010). Geochemical analyses were performed by Alex Stewart Assayers Argentina following the coding ICP-AR-42/OxM for sedimentary rock and ICP-MA-39/OxM for eggshell samples.

4. Descriptions

4.1. Geological setting

Although the Cretaceous Los Llanos Formation crops out in other regions of La Rioja Province, thus indicating that the basin was originally larger (perhaps more than 45,000 km^2), the 4-m-thick egg-bearing horizon in the uppermost section of this formation (Tauber, 2007; Grellet-Tinner and Fiorelli, 2010) has so far only been recorded in the Sanagasta Valley in the central region of the Sierra de Velasco. The nesting site is relatively small (ca. 300,000 m^2), mostly located within SGP boundaries in the Sanagasta Valley (see Grellet-Tinner and Fiorelli, 2010). The sediments of the egg-bearing outcrops (Fig. 2) overlie the laterally and vertically variable red Sauces Formation (Upper Palaeozoic,

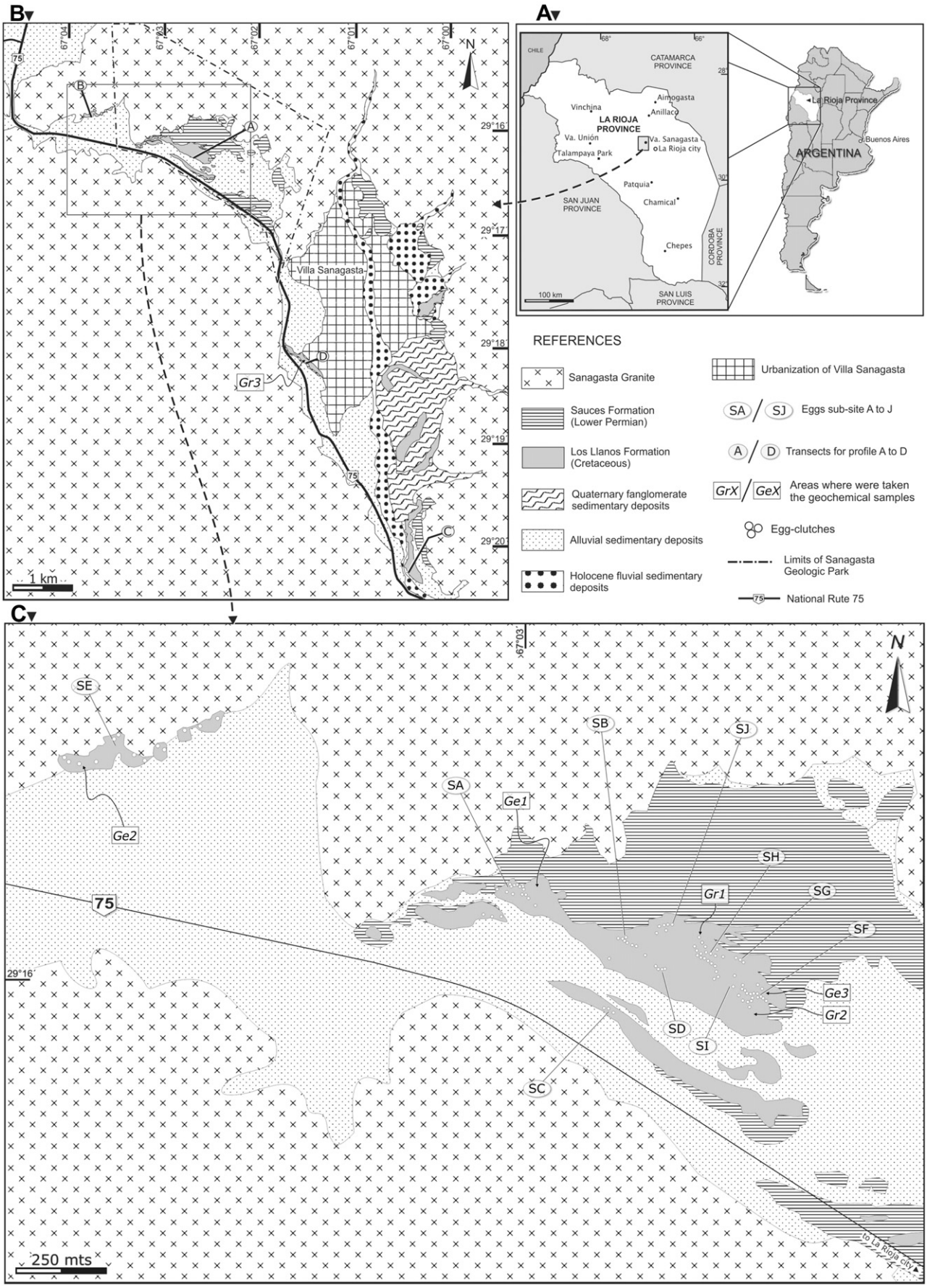
B
A
C
N
Villa Sanagasta
Gr3
1 km
29°16'
29°17'
29°18'
29°19'
29°20'
67°04'
67°03'
67°02'
67°01'
67°00'
75
CHILE
CATAMARCA PROVINCE
LA RIOJA PROVINCE
SAN JUAN PROVINCE
CORDOBA PROVINCE
SAN LUIS PROVINCE
Aimogasta
Vinchina
Anillaco
Va. Unión
Va. Sanagasta
La Rioja city
Talampaya Park
Patquia
Chamical
Chepes
100 km
La Rioja Province
Buenos Aires
ARGENTINA
REFERENCES
Sanagasta Granite
Sauces Formation (Lower Permian)
Los Llanos Formation (Cretaceous)
Quaternary fanglomerate sedimentary deposits
Alluvial sedimentary deposits
Holocene fluvial sedimentary deposits
Urbanization of Villa Sanagasta
SA / SJ Eggs sub-site A to J
A / D Transects for profile A to D
GrX / GeX Areas where were taken the geochemical samples
Egg-clutches
Limits of Sanagasta Geologic Park
National Rute 75
SE
Ge2
Ge1
SA
SB
SJ
SH
SG
SF
Gr1
Ge3
Gr2
SD
SI
SC
250 mts
to La Rioja city

Table 1
Summary of the oological and sedimentary samples used for palaeontological, petrographical and geochemical analyses.

Sanagasta sites	Clutches number	Clutches removed	Eggshell samples (*n*)[a]	Eggshell thin section	Petrographic thin section	Eggs geochem.[b]	Sediment geochem.[c]
Sub-site A	16	2	1026	Yes	Yes	Yes	No
Sub-site B	7	x	182	Yes	Yes	No	No
Sub-site C	2	x	121	Yes	No	No	No
Sub-site D	4	x	159	Yes	Yes	No	No
Sub-site E	11	2	386	Yes	Yes	Yes	No
Sub-site F	18	1	716	Yes	Yes	Yes	Yes
Sub-site G	2	1	50	Yes	Yes	No	No
Sub-site H	19	1	323	Yes	Yes	No	Yes
Sub-site I	3	x	111	Yes	Yes	No	No
Sub-site J	6	x	148	Yes	No	No	No

[a] Number of eggshell fragments used for statistical analysis, thin sections and geochemical analysis.
[b] Eggshell samples for geochemical analyses.
[c] Rock samples for geochemical analyses.

Paganzo Group) at a low angle, ubiquitous unconformity (Figs. 2, 3, 4A–C) (Tauber, 2007; Grellet-Tinner and Fiorelli, 2010). The upper levels display several types of brecciated palaeohydrothermal structures (e.g., vertical conduits, veins and pipes) that enter the uppermost horizontal strata (Fig. 4C). Recent palaeobotanical and palynological studies have restricted the age of the Sauces Formation to the early Early Permian (Pieroni and Georgieff, 2007). This formation, in turn, rests unconformably on the Sanagasta granite (see Figs. 2, 4C), a crystalline basement rock that consists of medium to coarse-grained, porphyritic texture and syeno- to monzogranite composition. U-Pb monazite dating indicates an Early Carboniferous crystallization age (353 ± 1 Ma; Grosse et al., 2009). The composition of the Sanagasta granite is SiO_2 (>70%) and K_2O (>4.9%), with weakly peraluminous (aluminium saturation index, ASI = 1.01–1.09), intermediate to high concentration ranges for High Field Strength Elements (HSFE) such as Y, Nb, Ga, Ta and Th, and relatively low Sr, Ba and Eu content (Grosse et al., 2009).

The Cretaceous Los Llanos Formation is characterized, in the SGP, by medium to coarse-grained grey, whitish, and yellowish arkosic sands (Fig. 4). However, the basal section consists of conglomerates with quartz lithoclasts, overlain by a highly cemented, very coarse-grained sandstone layer with interfingered pink claystone intraclasts. It presents in several places tabular and trough cross-bedding stratification of low angle or poorly defined horizontal stratification, interpreted by Tauber (2007) as interbraided river systems. Moreover, the basal level displays horizontally aligned calcite geodes and druses with bipolar growth (Fig. 4) that are associated with palaeohydrothermal discharge channels, cavities, and conduits (Immenhauser, 2009; Pirajno, 2009). In addition, the middle and upper section of the formation exhibits evidence for the former presence of numerous geothermal structures, chiefly vents, fountain geysers and hot springs together with long horizontal calcite veins, mini-dams, and fossil mud drainages and runoffs (Figs. 4, 6, 7).

The formation rests unconformably on the red and sandy Permian Sauces Formation (as noted above) infilling palaeochannel and large erosive surfaces that host several geothermal facies: (1) vertical carbonate breccia pipe-like structures cutting the horizontal red beds; (2) sub-vertical and diagonal calc- and silica veins (ca. 0.5 cm wide) exhibiting a “honeycomb” structure (Fig. 4C); (3) ubiquitous botryoidal silica-rich deposits, laminated opal-A cements and geyserites; (4) silica-rich geodes and druses and several siliceous sinters (microfacies) (Fig. 8), all of which can be readily observed in the Permian exposure.

Several types of geothermal structures are evident in the Los Llanos Formation at SGP: domed, terraced mounds, ponds, and travertine dam and mini-dam-like structures (Figs. 4, 6, 7, 9), similar to those described for the modern Norris Basin in Yellowstone National Park, USA (Guidry and Chafetz, 2003; Pentecost, 2005; Pirajno, 2009). In addition, there are typical minerals (siliceous sinters) associated with hot springs (Heaney, 1993; Sillitoe, 1993; Cady and Farmer, 1996; Carroll et al., 1998; Guidry and Chafetz, 2002; Konhauser et al., 2003), best exemplied by botryoidal quartz, chalcedonic crystals and green chrysoprase, which are ubiquitously distributed throughout the exposure. In fact, the egg-bearing horizon displays several singular microfacies of siliceous sinters (Fig. 8) resembling the siliceous microfacies of modern hydrothermal fields and hot spring deposits described by Schinteie et al. (2007). Small cup-shaped (ca. 0.5–5 cm Ø) siliceous sinters with a spicular edge, and plane and smooth flow, flat-shaped sinters (Grellet-Tinner and Fiorelli, 2010) are also very common (Fig. 8B, E). Such small microfacies, microstromatolith and microbialites (biosilicifications) grow and develop at the air–water and water–sediment interface (Campbell et al., 2002; Benning et al., 2005; Handley et al., 2005; Schinteie et al., 2007; Konhauser et al., 2008; Preston et al., 2008; Tobler et al., 2008) and are symptomatic, according to Schinteie et al. (2007), of relatively acidic (pH ~2.5) and low temperature (30 and 80 °C) hydrothermal activities.

Thin (ca. 5 mm Ø) silicified rhizoliths and rhizocretions including root cast and moulds are commonly observed in the upper level. They correspond to permineralized root systems replaced by chalcedony, opal, calcite and a clay mineral (aluminosilicate). According to Jones et al. (1998) and Owen et al. (2008), thermal fluids percolate and saturate the sediments (see also Pirajno, 2009) providing enough silica for the permineralization of plant tissues that is further concentrated by capillarity evapotranspiration. As such, the plant tissues act like a template for SiO_2 precipitation. Tissue decay increases CO_2 locally and lowers the pH (Jones et al., 1998; Channing and Edwards, 2004, 2009; Owen et al., 2008).

Fig. 1. Geographical and geological setting of the Sanagasta nesting site, at Sanagasta Geologic Park, La Rioja, Argentina. A, map of Argentina and La Rioja Province with the location of the Sanagasta valley. B, geologic map of the Sanagasta valley including the location of the Sanagasta Geologic Park and nesting site (A–D transects in Fig. 1B represent the stratigraphic profiles of Fig. 2, respectively). C, geologic and nesting map of the Sanagasta nesting site with the distribution and location of the sub-sites (SA–SJ, respectively) and egg clutches. Areas where rock (Gr1-3) and eggshell (Ge1-3) samples for geochemical analyses were taken are indicated. Codes for rock samples: Gr1, sample from sub-site H: SAN 1 (Upper Permian level, –uP–), SAN 2 (Lower Cretaceous horizon, –lK–), and SAN 6 (Upper Cretaceous horizon, –uK); Gr2, sample from sub-site F: SAN 3 (uP), SAN 4 (lK), and SAN 5 (uK); Gr3 sample from Los Barqutilos outcrop (see in B): SAN 7 (uP), SAN 8 (lK), and SAN 9 (uK). (For details of the stratigraphic column, see Fig. 3). Codes for eggshell samples: Ge1, SAN-SSA (from sub-site A); Ge2, SAN-SSE (from sub-site E); Ge3, SAN-SSF (from sub-site F).

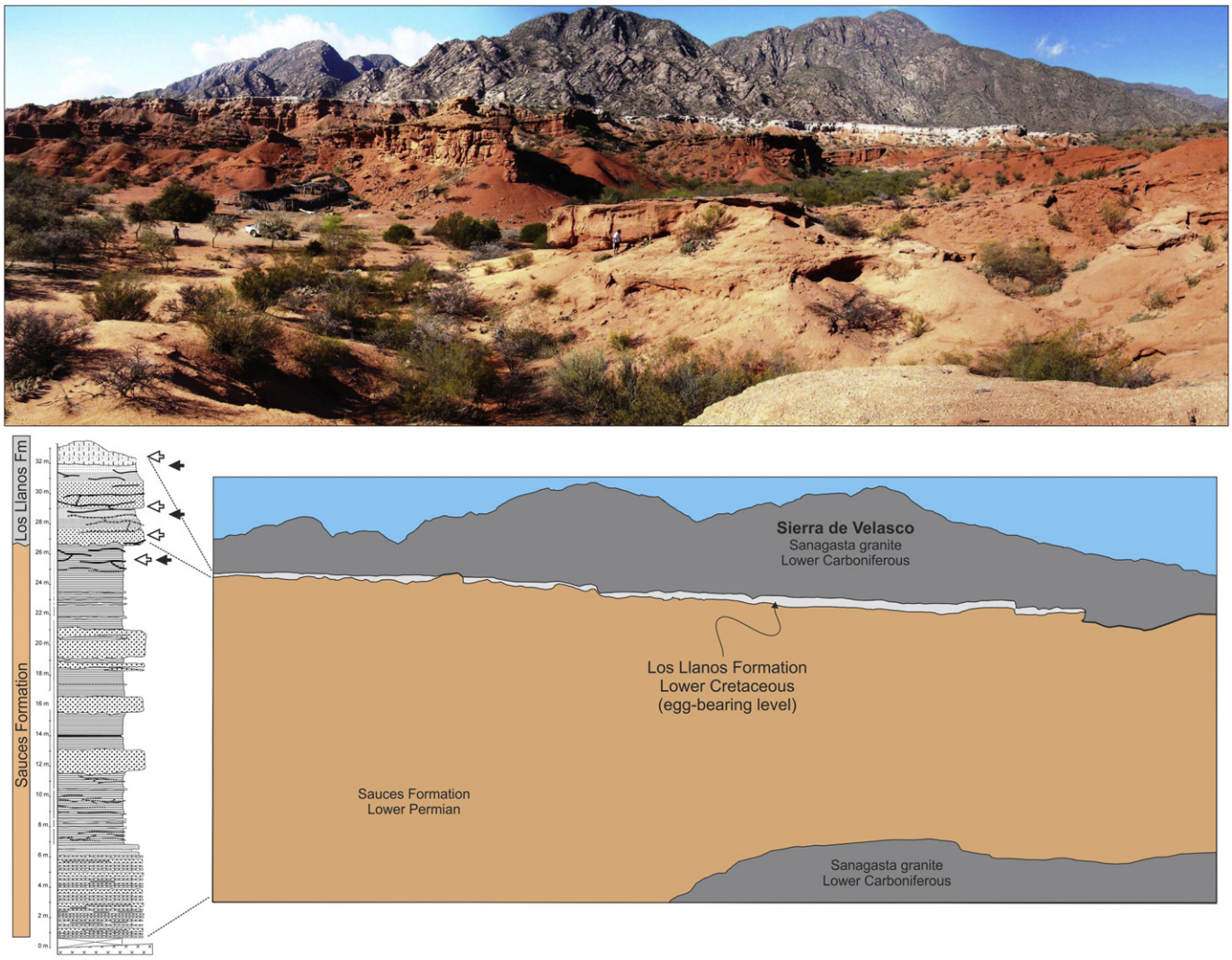

Fig. 2. Panoramic view of Sanagasta Geologic Park with the white Los Llanos Formation (egg-bearing level) above the red Sauces Formation with the Sierra de Velasco background. Arrows: levels where rock samples for petrographic (white arrows) and geochemical (black arrows) analyses were taken. (For details of the stratigraphic column, see the Fig. 3). (For interpretation of the references to colour in this figure legend, the reader is referred to the web version of this article.)

The upper Los Llanos Formation section is interspersed by numerous megastructures up to 30 m long that resisted erosion. They are devoid of any distinct stratification and consist of pebbly silcrete and calcrete sediments with conspicuous vents, mounds, large calcite geodes and druses, discharge channels, cavities, conduits, fountain geysers, and fossil mud drainages and runoffs with the presence of biomineralized (silicified) stromatolite filaments. All the egg clutches are located in and on these structures within 1–3 m of the geothermal deposits. Other surface geothermal expressions associated with the egg clutches are sub-circular (ca. 1–2 m diameter; see Figs. 6, 7) carbonate structures, mirroring exactly modern thermal or mud pools. The outer rims display several thin laminated microfacies (Fig. 7D–G) that, according to several authors, could correspond to micro-stromatolitic calcareous structures, fossil bacterial mats and microbialites (e.g., Cady and Farmer, 1996; Reysenbach and Cady, 2001; Rothschild and Mancinelli, 2001; Dupraz et al., 2009). Large calcite geodes and tubes with hefty bipolar growth, scalenohedric calcite crystals covering the internal walls of cavities are regularly observed in these megastructures (Figs. 4D, 7E).

The egg-bearing exposures outside, but adjacent to, the SGP at sub-site E (also called “Los Cajones” sensu Tauber, 2007) (see Fig. 1C) lack the underlying red Permian sedimentary levels of Sauces Formation; thus the egg-bearing sediments unconformably rest on the Sanagasta granitic basement (Grellet-Tinner and Fiorelli, 2010). The Cretaceous egg-bearing level represents, in fact, the entire sedimentation of the local hydrothermal system (Grellet-Tinner and Fiorelli, 2010 and reference therein). The mega-sedimentary calcareous structures at sub-site E are diverse, being composed of: (1) large hydrothermal mound or terrace levels; (2) several tube-like and conduit-like structures; (3) large calcite geodes (ca. 50 cm) (Fig. 4C, D); (4) thick and thin stratified travertine levels; and (5) calc-sinter structures with “mini-dam” patterns or “microterraces” (see Figs. 5, 6). The sub-site E outcrops (see Figs. 1C, 3 profile B, and 4G) lack siliceous structures and silica-microfacies like siliceous sinters, indicating a localized hydrothermal process of low temperature (<50 °C) and also possibly explained by the absence of Permian quartz-rich sandy sediments under the egg-bearing levels. Overall, the level is similar to that of the SGP outcrops in consisting of arkose/quartz-feldspar sandstones, partially conglomeratic, with grey calcareous cement (Tauber, 2007), the egg clutches occurring within about 2–3 m of the fossilized geothermal remains (Grellet-Tinner and Fiorelli, 2010). Interestingly, the egg-bearing layer (Fig. 9) is limited to

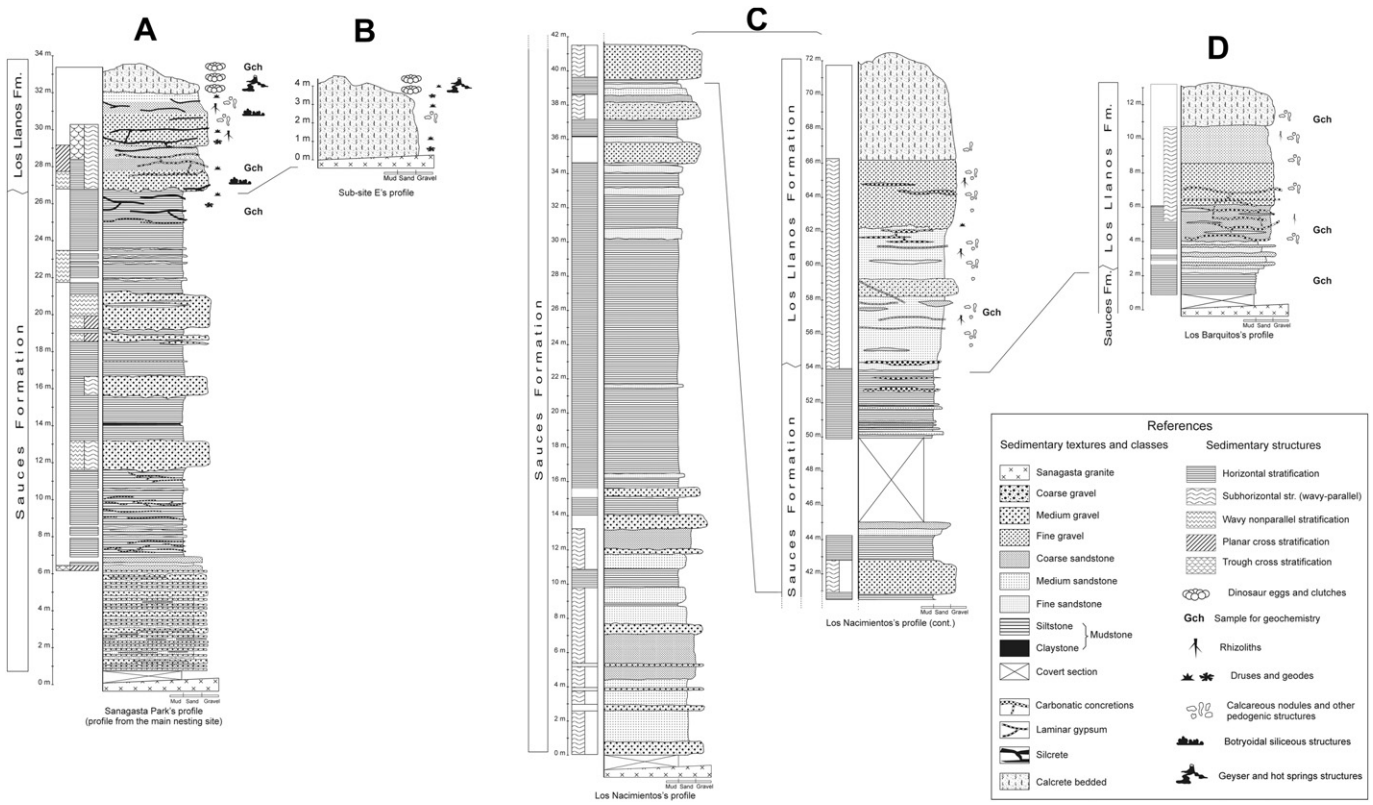

Fig. 3. The Cretaceous Los Llanos Formation. Stratigraphic profiles and correlations of the Sanagasta nesting site and related outcrops in the Sanagasta valley (columns A–D represent transects noted in the Fig. 1B, respectively). A, stratigraphic column of the Sanagasta Geologic Park at the main nesting site. B, stratigraphic profile for the outcrops at sub-site E (see Fig. 1B). C, stratigraphic column for the outcrop at the Los Nacimientos locality. D, stratigraphic column for the Los Barquitos locality close to Sanagasta village.

the SGP and sub-site E, where geothermal activities were documented, although the Los Llanos Formation frequently surfaces in other parts of the region. The clutches were confined within an inter-mountain microbasin a few kilometres long that was furrowed by meandering "warm" rivers in an unusual fluvial system (Grellet-Tinner and Fiorelli, 2010). The numerous egg clutches are exclusively found in the silcrete-calcrete structures, which averages 1.5 m thick within the SGP and resembles, in several respects, the South Korean egg-bearing geological setting of the Seonso Formation in the Gyeongsang Basin (Paik et al., 2004; Kim et al., 2009a). In fact, the Seonso nesting sites are characterized by an Andean-type continental margin, similar to that of Sanagasta, and display synchronous geotectonic and igneous activity with numerous palaeohydrothermal deposits (Choi, 1986; Chough et al., 2000; Lee and Lee, 2000; Choi et al., 2005a; Hwang et al., 2008, and discussions therein).

4.2. Petrographic overview and microsedimentology of the egg-clutch level

The horizontally variable sediments at the nesting site are characterized by very coarse sandstones and conglomerates that display microfacies and microfabric changes within a few centimetres. In thin section, the sandstone grains are sub-rounded and well sorted, but poorly packed with a large amount of calcareous cement. In addition, well-packed, angular conglomeratic sandstones with a poorly sorted silicified matrix are also common. Irrespective of this, the egg-bearing level is classified as a typical arkose with sub-rounded to subangular clasts of low sphericity, implying an immature rock (Pettijohn et al., 1987) possibly regarded as a "wackestone" (sensu Dunham, 1962 and Wright, 1992). The brecciated pipes and carbonaceous conduits in the upper section of the Sauces Formation, and the domal, mound, and pond structures in Los Llanos Formation display a typical microfabric of hydrothermal shallow channels showing fossil biofilms and microbialite framestone (Fig. 10C–E). The sediments associated with the egg clutches have a low proportion of feldspars, lithocalsts and intraclasts (<15%) but a dominance of microcrystalline and polycrystalline quartz grains, along with a few chert grains (Figs. 11, 12A–D). The feldspars are represented by plagioclase, microcline (Fig. 11B), and pertites in lesser proportion. Although rare, the lithic fragments in the egg-bearing levels are made up of plutonic and sedimentary fragments from the Permian with heavy minerals such as apatite, zircon, rutile, tourmaline, and some opaque minerals (perhaps iron oxides and framboids). The grains and lithoclasts do not exhibit distortion, pressure, dissolution or recrystallization, but they do display micritization, corrosion, and wear derived from the diagenetic-hydrothermal environment (Figs. 11C, D, 12E, F). The calcite cement is very fine, granular with high relief and interference colour (Figs. 11, 12A, B). As such, the rock is regarded a sandstone with a carbonate-mud matrix (Fig. 11D, E; Adams and MacKenzie, 1998; Scholle and Ulmer-Scholle, 2003). The sparry cement (intrasparite) (Fig. 11) comes from an original micrite (intramicrite) (sensu Folk, 1962). This microsparite cement suggests a sedimentary process under conditions that led to the removal of the mud matrix, such as fast-flowing areas on the river bed, or slow-flowing but agitated areas (see Arenas-Abad et al., 2010); however, this calcite cement could also have formed from old caliche by recrystallization of a primary micrite (microcrystalline calcite) during diagenesis (Boggs, 1992). In addition, the rock displays a typical diagenetic-hydrothermal microfabric with silicate cement (mainly chalcedony and microchert) infilling voids (Figs. 11A, 12C–E). This siliceous phase is evidence of pre-compacting cement and an earlier episode of diagenesis in a hydrothermal

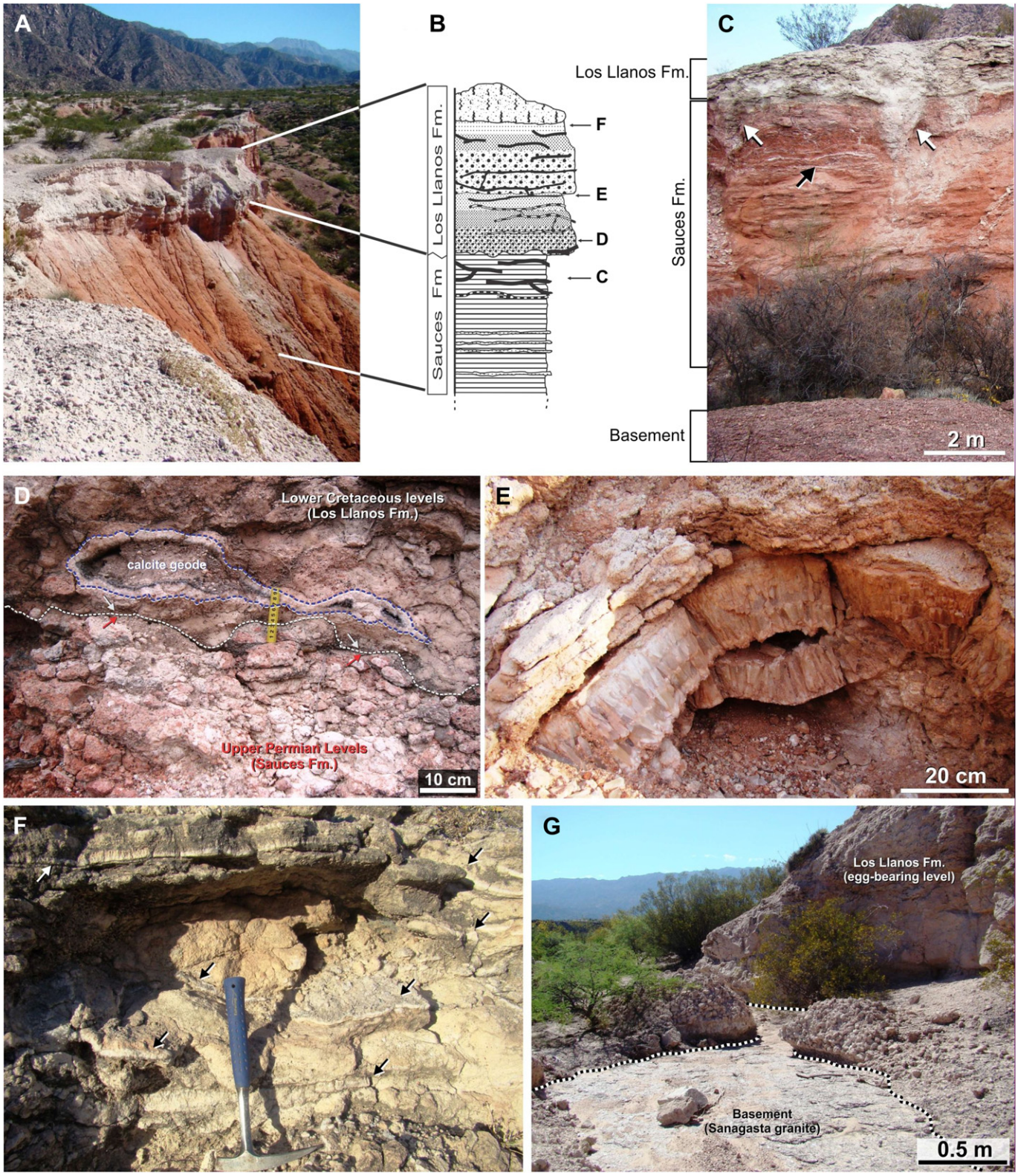

Fig. 4. Sedimentary and hydrothermal structures present in the Permian and Cretaceous formations. A, panoramic view of Sanagasta Geologic Park showing the white Cretaceous Los Llanos Formation overlying the red early Early Permian Sauces Formation. B, simplified stratigraphic profile of the nesting site. C, boundary between Permian and Cretaceous levels displays vertical brecciated pipe-like calcareous structures (white arrows) and silica-carbonate veins (black arrow). D, large calcite geode formed with "dogtooth" crystals (arrows and dotted line shows the P/K boundary). E, irregular geode of typical hydrothermal discharge channel or conduit formed by scalenohedron calcite crystals (see Immenhauser, 2009). F, large horizontal veins of scalenohedron calcite crystals (similar to the apron and pond facies; see Fouke et al., 2003; Veysey et al., 2008), relics of Cretaceous hot spring terraces and hydrothermal activities in the Sanagasta Geologic Park. G, sub-site E where the Cretaceous sediments of the Los Llanos Formation rest directly on the granitoid basement (dotted lines shows the basement/Cretaceous boundary). (For interpretation of the references to colour in this figure legend, the reader is referred to the web version of this article.)

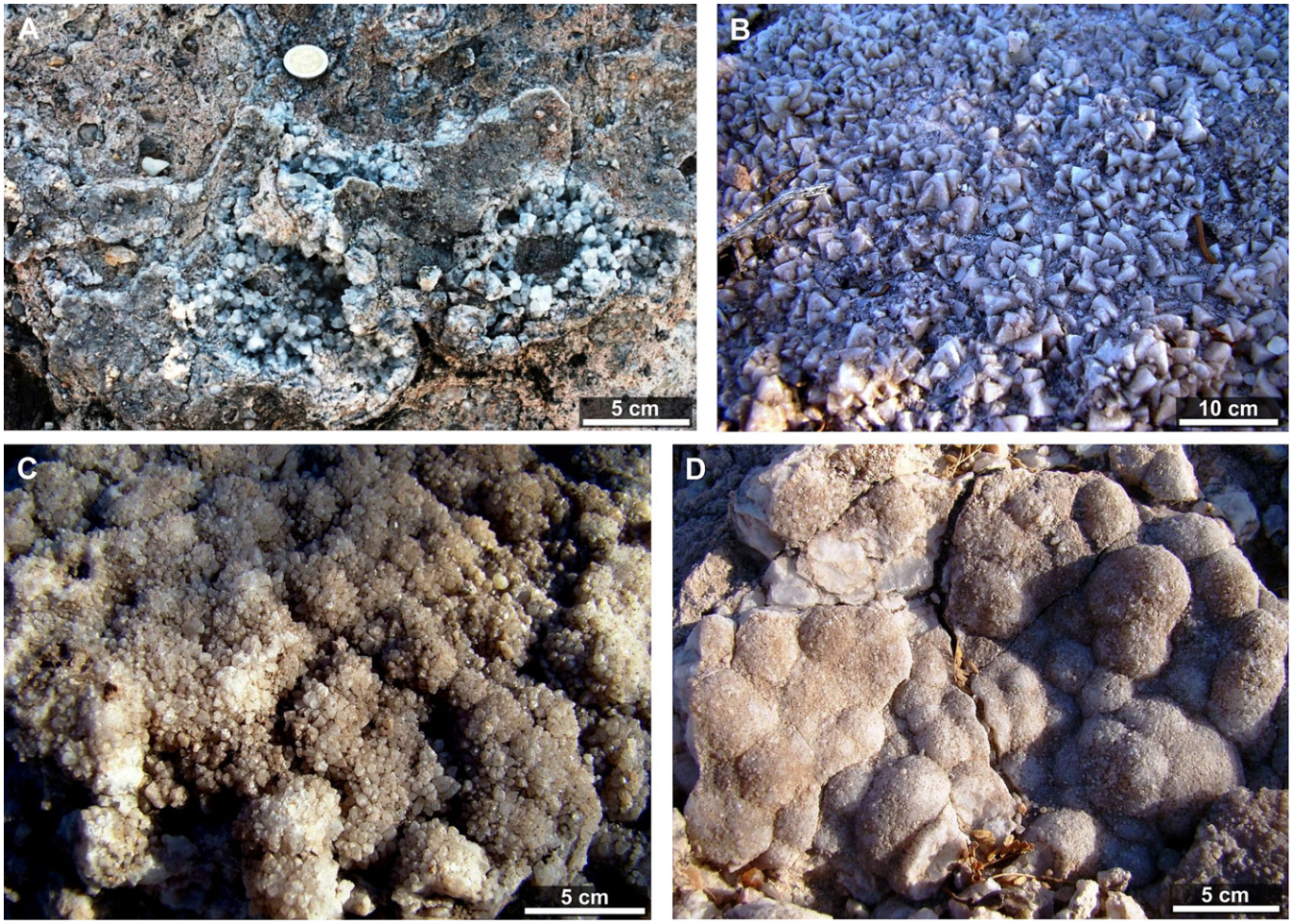

Fig. 5. Cal-sinter structures and facies at Sanagasta Geologic Park. A, blue calcite crystals of a "mini-dam"-like structure from proximal and distal slope facies. B, large pyramidal crystals from runoffs and proximal facies of a geyser. C, mini-crystal calcite from runoffs and pond facies. D, botryoidal calcite with microcrystals perhaps from pond facies. (For interpretation of the references to colour in this figure legend, the reader is referred to the web version of this article.)

environment. Although, the porosity is primary intergranular (interparticle) (sensu Choquette and Pray, 1970), the rock displays a secondary intergranular porosity (Figs. 11, 12). However, the partial recrystallization of the fossils (Fig. 11) and some infilling of spaces by drusy calcite cement and quartz (mainly chalcedony) (Figs. 11D, E, 12E) also suggest secondary intragranular and intergranular porosities. Therefore, the immature rock, the microfabric of shallow hydrothermal channels, the micritization and corrosion of grains, the sparry and silicate cements, and hydrothermal eodiagenesis indicate, and are congruent with, substantial and prolonged geothermal activity.

4.3. Palaeohydrothermal structures and microbialite petrography

The calcite crystals in conduits and pore voids produced by hydrothermal fluids have a filamentous appearance or are represented by equigranular and palisade cements (Fig. 12; see Scholle and Ulmer-Scholle, 2003). Moreover, the hot springs and geyser structures present particular silicate (Fig. 13B) and carbonate cementation patterns with bipolar, palisade growth, calcitic crystals (Fig. 13D) through several phases as documented by Immenhauser (2009; see also Muchez et al., 1998; Suchy et al., 2000; Nielsen et al., 2005; Flügel, 2010). The Cretaceous sedimentary level, associated with the megastructures, displays several calcareous slope microfacies and microbialite framestones formed by silicified filamentous stratified and laminated "crust-like" microstromatolites (Fig. 14A–D), and cyanobacteria filaments (e.g., cf. *Calothrix*) (Figs. 10E, 14E), with a matrix composed of fossil "pinnate" diatoms (Fig. 14A, C, F). The silica in the epithermal environment is mainly derived from alumino-silicates and quartz (Pirajno, 2009), which are very common minerals in the Sanagasta granite (Grosse et al., 2009) and the Permian sediments (Pieroni and Georgieff, 2007; Grellet-Tinner and Fiorelli, 2010). In thin section, the siliceous microfabrics fill up voids, replace sections of the calcareous cement, and display euhedral quartz crystallites, drusy mega-quartz mosaics, microcherts, chalcedony cements, fibrous silica and opals (Figs. 10C, 12C–E, 13). The same siliceous microfabrics could also be observed in colourful botryoidal silica macrostructures (Fig. 8D). Epidote aggregates (mainly replacing sections of the fossil eggshells) is a common sorosilicate mineral that may have a secondary origin by hydrothermal alteration of plagioclase through a "saussuritization" process (see discussion below).

Hydrothermal mineral phases that develop in epithermal systems are dependent on temperature, pressure, rock type, nature of the circulating fluids (such as pH, presence of CO_2 and H_2S) and water/rock ratios. At lower temperatures (<180 °C) the common mineral phases related to geothermal fluids are calcite, kaolinite, smectite, cristobalite, gypsum, opal, quartz, and epidote (see

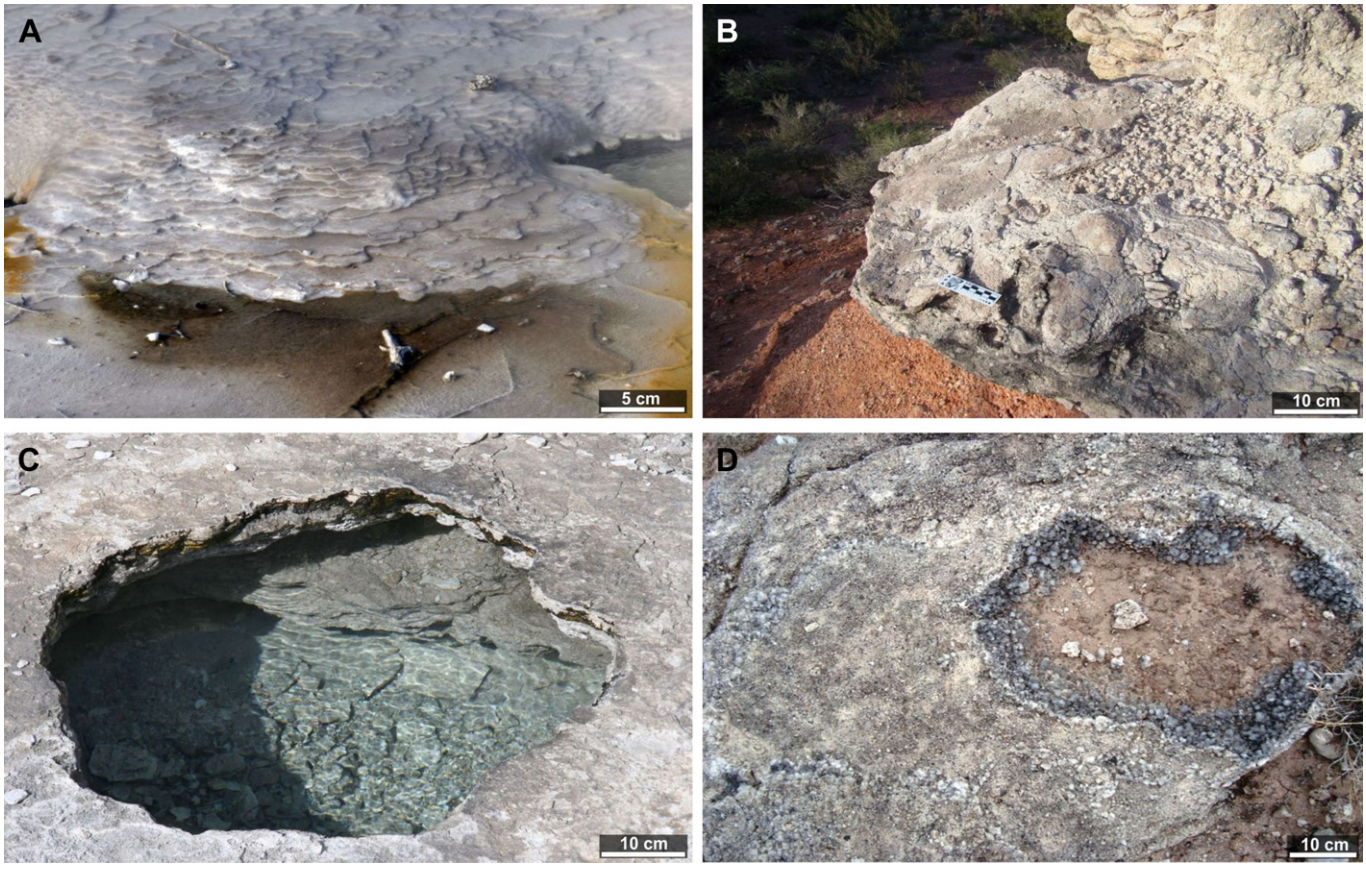

Fig. 6. Comparison between the Norris Basin in Yellowstone National Park (A and C) and the Sanagasta Geologic Park nesting site (B and D) hot-spring structures. A, B, calcareous mud drainages ("mini-dams") and runoffs from slope facies. C, D, thermal-pool and hot-spring structures.

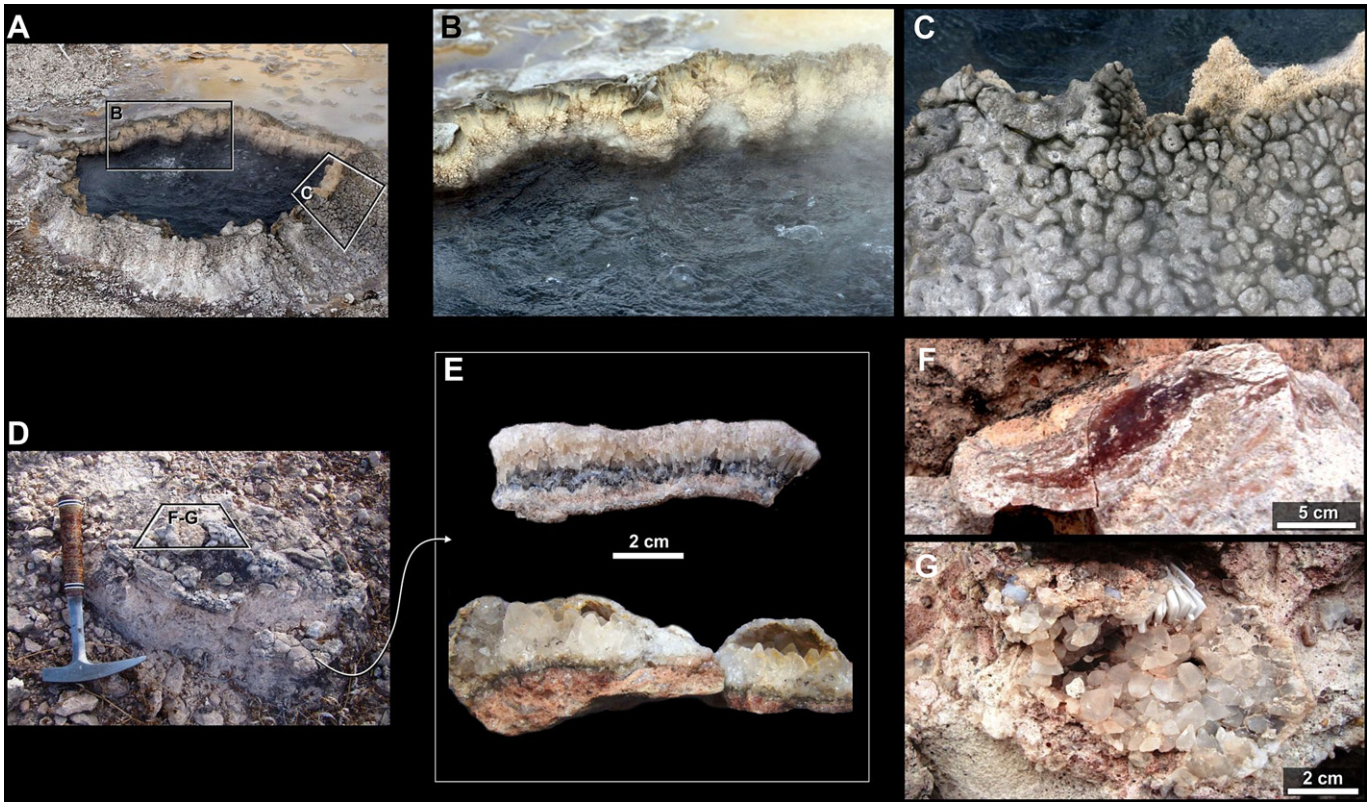

Fig. 7. Comparison between the Norris Basin in Yellowstone National Park (A–C) and the Sanagasta Geologic Park nesting site (D–G) hydrothermal structures. A, geyser. B, C, edges of the geyser displaying microbialites and biofacies. D, palaeo-hot spring (mound-like) structure; microbialite, laminated microfacies and micro-stromatolitic calcareous structures from the edge of the palaeogeyser. F, fine pink travertine microfacies. G, scalenohedron (dog-tooth spar) and rhombohedron calcite crystal microfacies from the centre of a fossil geyser pool. (For interpretation of the references to colour in this figure legend, the reader is referred to the web version of this article.)

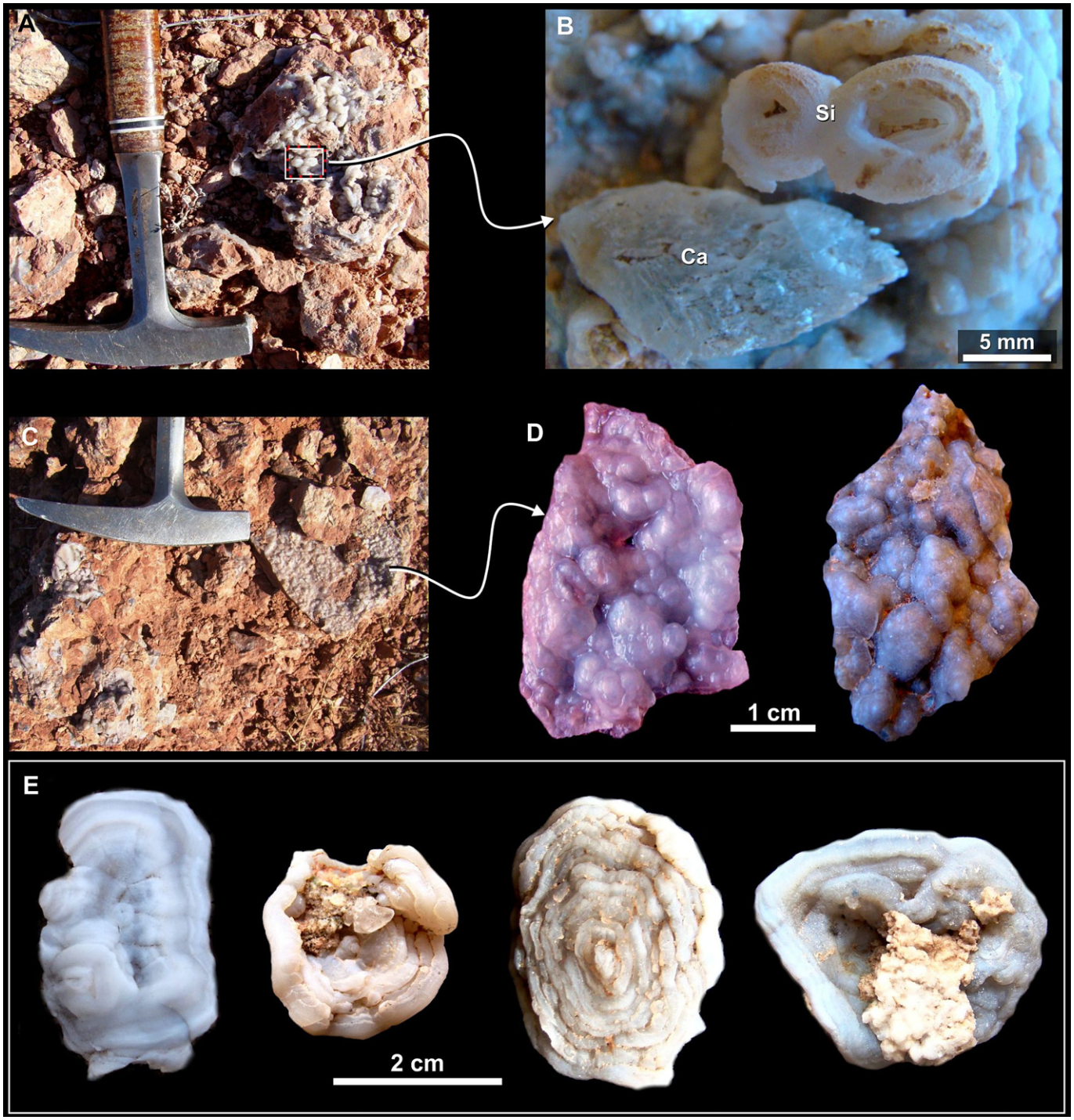

Fig. 8. Siliceous-sinter microfacies from the Sanagasta nesting site. These ubiquitous sinters, commonly deposited by hydrothermal solutions either in channels or on surfaces near vents, add another level of support to past hydrothermal activity in the Sanagasta Valley. A, C, in-situ siliceous-sinter microfacies at the P/K boundary. C, D, magnification of A and C, respectively, showing small cup-shaped (C) and botryoidal (D) silica sinters. E, small siliceous microfacies which are ubiquitous at the nesting level and associated with the egg clutches indicate temperatures of ca. 40 °C for the palaeothermal fluids between the clutches. Abbreviations: Si, siliceous sinter; Ca, calcite crystal.

Pirajno, 2009, p. 121). Most of these phases are represented in the sediments and fossil eggs at the Sanagasta nesting site, thus reinforcing the concept that the egg-bearing level was formed and concomitantly altered by an epithermal system at shallow depths and relatively low temperatures (<180 °C) and pressures (see e.g., White and Hedenquist, 1990; Browne, 1991; Pentecost et al., 2003; Renaut and Jones, 2003; Pirajno, 2009).

4.4. Brief description of the clutches and eggs at the nesting site

Nesting site and clutches. Throughout the SGP, the egg clutches are below, above, and at the same levels as the vents, fountain geysers and geothermal mounds indicating a substantial period of coeval and associated geothermal and ovideposition activities. Although each clutch is easily identified by a regularly distributed

Fig. 9. Comparison between the Norris Basin in Yellowstone National Park and the Sanagasta Geologic Park. A, C, E; hydrothermal structures (conduits, geysers and mounds) in the Norris Basin. B, D, F, hydrothermal structures at the Sanagasta Geologic Park nesting site. A, B, large calcite crystals (dog-tooth-like) with bipolar growth in the cavities of conduits and pipes. C–F, typical mounds and hydrothermal vents structures.

number of eggs within a defined area and volume, no nest structures or architectures with sedimentary rims were noted. The clutches consist of up to 35 eggs but the most consist of 3–12 eggs because of taphonomic processes and recent natural and anthropogenic weathering (Fig. 15). Clutches with more than 30 complete eggs rest on a surface 1.8 m^2 with a maximum clutch axis of 220 cm (Grellet-Tinner and Fiorelli, 2010). The three-dimensional clutch geometry is well preserved, showing two egg rows, with more eggs in the upper row. This possibly reflects laying patterns and behaviours, with the spatial distribution implying a deliberately excavated hole as a nesting structure rather than eggs having been deposited on the surface (Fig. 15A–C).

The eggs and eggshells. Although described by Grellet-Tinner and Fiorelli (2010), we recapitulate here the main egg and eggshell characters. The subspherical and slightly ovoid eggs average 21 cm in diameter (min 20 cm, max 23 cm), their circumference is 61–63 cm, and their maximum volume is estimated to be 6370 cm^3 (Grellet-Tinner et al., 2012). The mono-layered eggshell displays thickness variations, which are visible on a single egg and

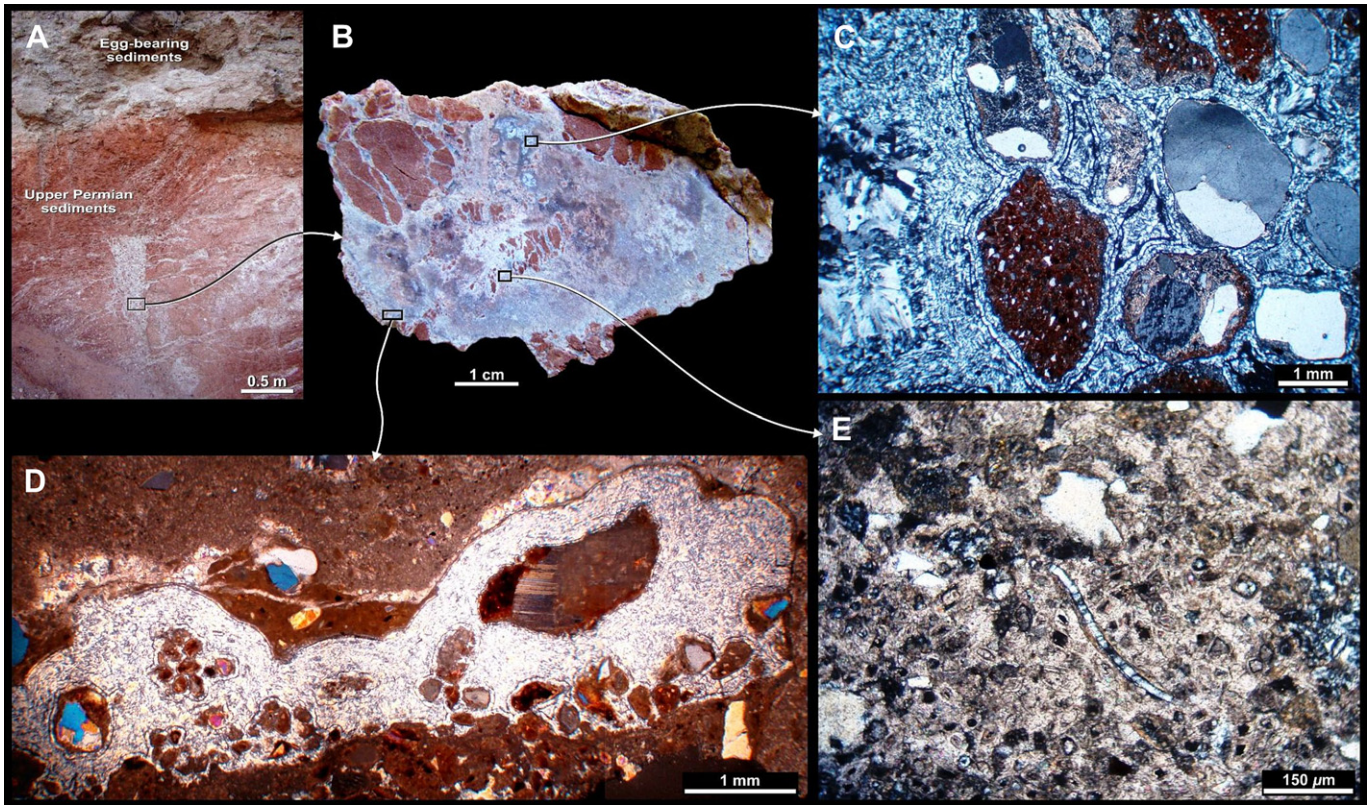

Fig. 10. Palaeohydrothermal structures and microfabrics from the P/K boundary. A, Late Permian sediments showing a pipe-conduit structure. B, rock fragment at the same level with characteristic hydrothermal lithology. C–E, petrographic thin sections of B. C, typical hydrothermal microfabric with chalcedony and silicified microstromatolite filaments forming the rock matrix and embedding completely the rock fragments and quartz grains. D, silicified microstromatolite infilled the sediment associated with a red Permian lithoclast. E, photomicrograph of a silicified microbial filament (cf. *Calothrix*), a typical cyanobacterian from ancient and modern hydrothermal systems preserved in the calcareous rock microfabric. (For interpretation of the references to colour in this figure legend, the reader is referred to the web version of this article.)

were noted in all sub-sites to be from 1.29 to 7.93 mm, with a mean thickness of 3.847 mm ($n = 3077$). Rounded or sub-rounded to sub-polygonal nodular structures on the surface average 0.629 mm in diameter with a significant variation ($X = 2{,}94$ node per mm^2). No alleged pathological eggshell fragments with two or more layers were recovered. The eggshell unit nuclei are only observed in very few cases and are generally poorly preserved. In shells thicker than ca. 2.5 mm, the eggshell units display secondary dichotomic or polytomic ramifications which developed as they grew outwards. The abundant pore canals exhibit different morphologies that vary according to the thickness of the shell. They are notably straight with a greater diameter towards the innermost eggshell surface in thin shells, but meander with several dichotomous ramifications towards the outermost shell surface in the thick shells. The pore aperture diameters average 0.1854 mm with a concentration of 5.86 p/mm^2. From a parataxonomic perspective, the thinner eggs would be assigned to the traditional parataxonomic oofamily Megaloolithidae (Zhao, 1979) with a discretispherulitic eggshell structure, compactituberculate surface morphology, and tubocanaliculate pore system. However, the thicker shell would be attributed to Faveoloolithidae (Zhao and Ding, 1976) with a filispherulitic morphotype and multicanaliculate pore system. This inconsistency is related to the shell thickness, itself influenced by chemical erosion of the outer shell (Grellet-Tinner and Fiorelli, 2010) coupled with the vagaries of dinosaur eggshell parataxonomic classification, because monospecific eggs cannot belong to two different (artificial) oofamilies.

4.5. Geochemical analyses of eggshell and sediment

This section recapitulates and expands upon the geochemical analysis of sediments and fossils reported by Grellet-Tinner and Fiorelli (2010) not only to understand better the unique relationship between the nesting behaviour of the Sanagasta neosauropods and the geology of the nesting site, but also to determine the age of both processes. Sedimentary samples were collected from the same horizons at three different locations in the Sanagasta valley: two within the SGP (at sub-sites H and F) and another outside the park at Los Barquitos (profile D; see Figs. 1, 2) where no egg clutches and geothermal structures are present. The specimens were sampled in the: (1) upper level of the Sauces Formation (very fine-grained sandstone); (2) lower level of the Los Llanos Formation (very coarse-grained sandstone to conglomerate); and (3) upper level of the Los Llanos Formation (medium-grained sandstone), where the egg clutches were recovered. The SiO_2 concentration from the upper level of the Sauces Formation is ubiquitously high (between 70 and 83 wt.%). A similar SiO_2 concentration, but with a larger range was recorded from the lower and upper levels of the Los Llanos Formation at the sub-sites H and F (between 64 and 85 wt.%) except for one sample from the upper level of this formation (SAN 6, sub-site H), which displayed a lower value (32 wt.%). Overall, the samples from the Los Llanos Formation at the Los Barquitos locality (SAN 8 and 9, profile D in Fig. 2) display lesser SiO_2 values (54 and 59 wt.%) than those located in the nesting area. The calcium oxide results are similar to those of the silica in demonstrating anomalies for sub-sites H (values of 1.15–1.06, 35.87 wt.%) and F (9.14–15.81,

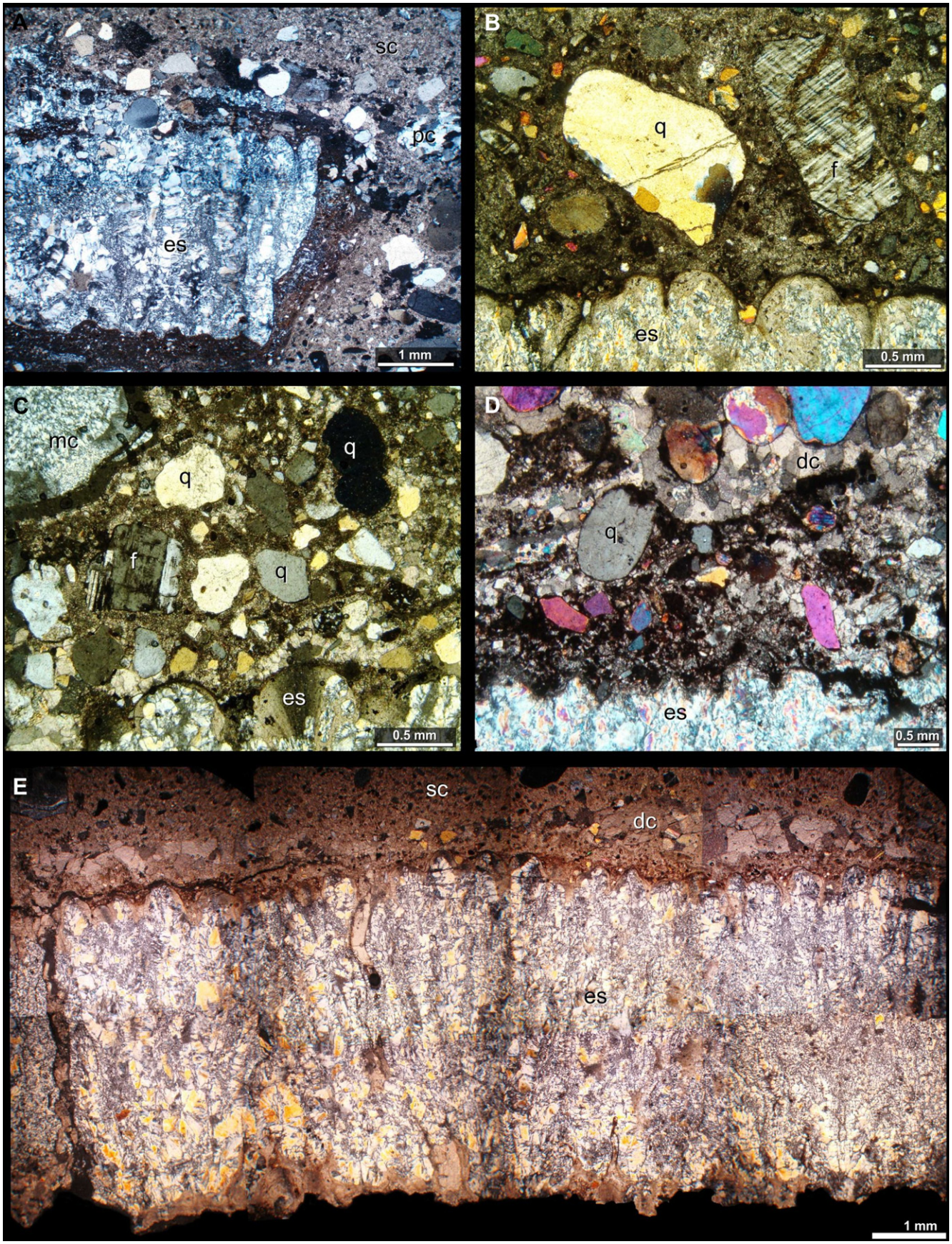
A
sc
pc
es
1 mm
B
q
f
es
0.5 mm
C
mc
q
q
f
q
es
0.5 mm
D
dc
q
es
0.5 mm
E
sc
dc
es
1 mm

8.82 wt.%) for the upper level of the Sauces Fm and lower and upper levels of the Los Llanos Formation, respectively (Table 2), whereas the levels at the Los Barquitos locality do not exhibit these anomalies (0.90 wt.% for the upper level of the Sauces Fm; 17.34 wt.% for the lower level and 16.61 wt.% for the upper level of the Los Llanos Formation). The concentration of Al_2O_3, TiO_2, Fe_2O_3, MgO, MnO, Na_2O, K_2O and P_2O_5 do not show significant variations among the studied samples (Table 2). Conversely, the concentration of trace elements varies widely. The upper level of the Sauces Formation at sub-sites H and F displays similar concentrations of V (52–59 ppm), Cu (18–28 ppm) and As (5–11 ppm), but higher values of Li, Ba, Pb, Zn at the sub-site H (Li = 19, Ba = 506, Pb = 19 and Zn = 46 ppm) than the sub-site F (Li = 6, Ba = 98, Pb = 4 and Zn = 12 ppm) (Table 2). However, at Los Barquitos, the Sauces Formation exhibits generally lower values (V = 15, Cu = 10, As < 5, Li = 7, Ba = 33, Pb < 2 and Zn = 10 ppm). A similar geochemical pattern is present in the Los Llanos Formation, where at the lower level of this formation, the highest concentrations are at sub-site H (Li = 9, Ba = 395, V = 93, Cu = 23, Zn = 17, Pb = 7 and As = 12 ppm) and sub-site F (Li = 3, Ba = 48, V = 10, Cu = 11, Zn = 4, Pb = 2 and As < 5 ppm) and lower at Los Barquitos (Li = 4, Ba = 24, V = 10, Cu = 8, Zn = 4, Pb < 2 and As < 5 ppm). Similarly, the upper level (egg horizon) of the Los Llanos Formation exhibits relatively higher values at sub-site H (Li = 5, Ba = 70, V = 18, Cu = 9, Zn = 6, Pb = 3 and As = 10 ppm) and lower values in the other profiles (sub-site F, Li = 4, Ba = 47, V = 12, Cu = 10, Zn = 5, Pb < 2 and <5 ppm; Los Barquitos, Li = 4, Ba = 65, V = 9, Cu = 8, Zn = 4, Pb < 2 and As < 5 ppm). All this suggests that the H (mainly) and F sub-sites were altered compositionally by hydrothermal/geothermal activities, in contrast to Los Barquitos where geothermal evidence such as geodes, druses, calcitic crystals, and geyserites botryoidal structures are absent (Fig. 16). Chemical analyses of eggshells from the A, E and F sub-sites (Fig. 1, Table 2) indicate low concentrations for all of the oxides except for CaO and SiO_2. Two eggshells display similar oxide contents (CaO = 30.84 and 32.49 and SiO_2 = 36.46 and 40.15, respectively) while the third has lower CaO (7.09 wt.%) and higher SiO_2 (80.61 wt.%) values, reflecting a higher degree of silicification. Similar trace element contents of the sedimentary rocks were recovered in the eggshells, with relatively anomalous values of Ba (from 33 to >2000 ppm), V (from 17 to 34 ppm) and lower concentrations of Pb (<2–5 ppm) and Zn (from 2 to 6 ppm). This geochemical similarity between the sedimentary rock and the eggshells implies that both were subjected to the same geothermal regime and alteration.

4.6. Cretaceous age for the egg-bearing level and Los Llanos Formation

Although recent work constrained the age of Los Llanos Formation to the Miocene (Ezpeleta et al., 2006; Ruskin, 2006; Dávila et al., 2007; Ruskin et al., 2011), the discovery of Cretaceous oological dinosaur remains reported originally by Tauber (2007), and subsequently confirmed by the discovery of the neosauropod nesting site at Sanagasta (Grellet-Tinner and Fiorelli, 2010), has necessitated a return to the original Cretaceous age determined by Bodenbender (1911). The eggs correspond to faveoloolithid type, which were laid by sauropod dinosaurs according to Tauber (2007) and Grellet-Tinner and Fiorelli (2010). The relationship between ovipositions and hydrothermal activity implies that both biological and geological processes were synchronous because the eggs were laid in hydrothermal ground. This implies a similar age because hydrothermal activity leads to rapid sediment lithification in weeks or months (see Guidry and Chafetz, 2003; Renaut and Jones, 2003; Pentecost, 2005; Pirajno, 2009). To sum up, the discovery of new Cretaceous fossils at the type locality of Los Llanos Formation (Fiorelli et al., 2011) supports Bodenbender's (1911) Cretaceous age determination. Based on the geochemical analyses, we propose here an Early Cretaceous age for the Sanagasta nesting site and Los Llanos Formation (see discussion below).

5. Discussion

Although previously faveoloolithid eggs were associated by some authors with titanosaurs (e.g., Casadío et al., 2002; de Valais et al., 2003; Simón, 2006), a lower taxonomic identity to Neosauropoda would provisionally be advisable without supportive evidence from fossil embryos "in ovo" (Grellet-Tinner and Fiorelli, 2010). This taxonomic association rests on both the oological characters indicating a sauropod affiliation (see Grellet-Tinner and Fiorelli, 2010; Grellet-Tinner et al., 2011) and the documented presence of both diplodocoid and titanosaurid sauropods in the fossil record of South America during that period of time (Grellet-Tinner et al., 2012). The taphonomy of this monotypic nesting site displays biostratinomic and fossil diagenetic pecularities. The three-dimensional spatial arrangement of the egg clutches dispersed throughout the entire egg-bearing horizon and geothermal relics implies that egg ovideposition and geothermal activity were coeval. Moreover, the ubiquitous presence of clutches within a radius of 3 m from a given geothermal relic may indicate a deliberate parental choice to ovideposit their eggs at these precise sites. Eggs were buried in the geothermal sediments before their consolidation and lithification. Hydrothermal sediments can be lithified rapidly within months (see Renaut and Jones, 2003; Scholle and Ulmer-Scholle, 2003; Pirajno, 2009), which is congruent with synchronization between oviposition and geothermal activity. The biocoenosis corresponds to a biogenic production of eggs, with eggshell mineralization altered by hydrothermal activity and biolithificating extremophile microorganisms (stromatolites, cyanobacteria, and diatoms; Fig. 14). Biostratinomy, thanatocenosis and time-averaging were virtually nil because the eggs were buried in the substrate after their ovideposition (Grellet-Tinner and Fiorelli, 2010). In contrast, the taphocenosis (buried associations) represents the most important taphonomic feature. The eggshells display several taphonomic alterations (e.g., high fragmentation, chemical erosion, and eggshell thinning) produced by acidic solutions immediately after oviposition, while re-calcification and silicification (mainly microsparite, chalcedony, microchert, opal-A, and epidotes) during the eodiagenesis are the most common eggshell recrystallizations. The presence of opal-A/CT microspheres ca.10 μm in diameter (see Grellet-Tinner and Fiorelli, 2010), epidote aggregates (e.g., clinozoisite through the "saussuritization" process), and fibrous clay minerals (e.g., smectite derivates from plagioclase through the

Fig. 11. Photomicrographs of sedimentary rocks with eggshell fragments from the Sanagasta nesting site. A, arkosic sandstone with eggshell fragment eroded and silicified by warm, acidic hydrothermal fluids. B, typical conglomeratic sandstone with large grains (quartz and feldspars) rounded by calcareous cement. C, D, sedimentary rocks with eggshell fragments under a petrographic microscope and cross nicols displaying different types of calcite cements and peloids (dark zone in D). E, very silicified complete eggshell with characteristic sedimentary sparry calcite cement. Abbreviations: ch, chalcedony; dc, drusy cement (equigranular); es, eggshell; f, feldspars; mc, microchert; pal, palisade; pc: polycrystalline; q, quartz grain; sc, sparry calcite cement.

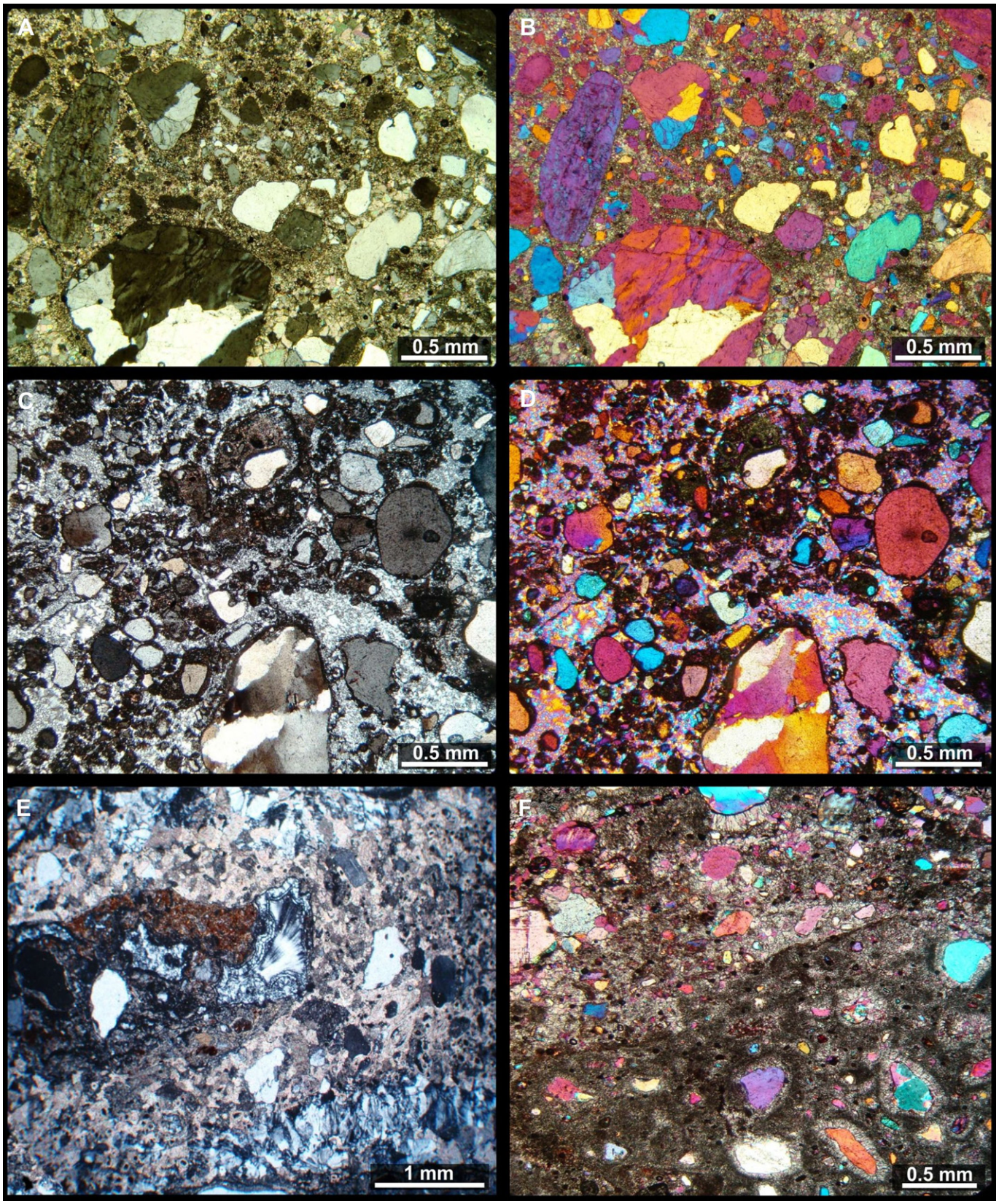

Fig. 12. Photomicrographs of the arkosic and conglomeratic sandstone from the egg-bearing level. A, B, quartz grains and calcareous (sparry) cement under a petrographic microscope and cross nicols (A) and cross-polarized light (B), C, D, arkosic and conglomeratic sandstone with a typical hydrothermal microfabric displaying a silicified (microchert and chalcedonitic) cement under cross nicols (C) and cross-polarized light (D). E, thin section from the Lower Cretaceous levels showing calcite and silicified cement infilling some pore spaces under cross nicols. F, sandstone with sparry calcite cement and palisade cement around the quartz grains in cross-polarized light.

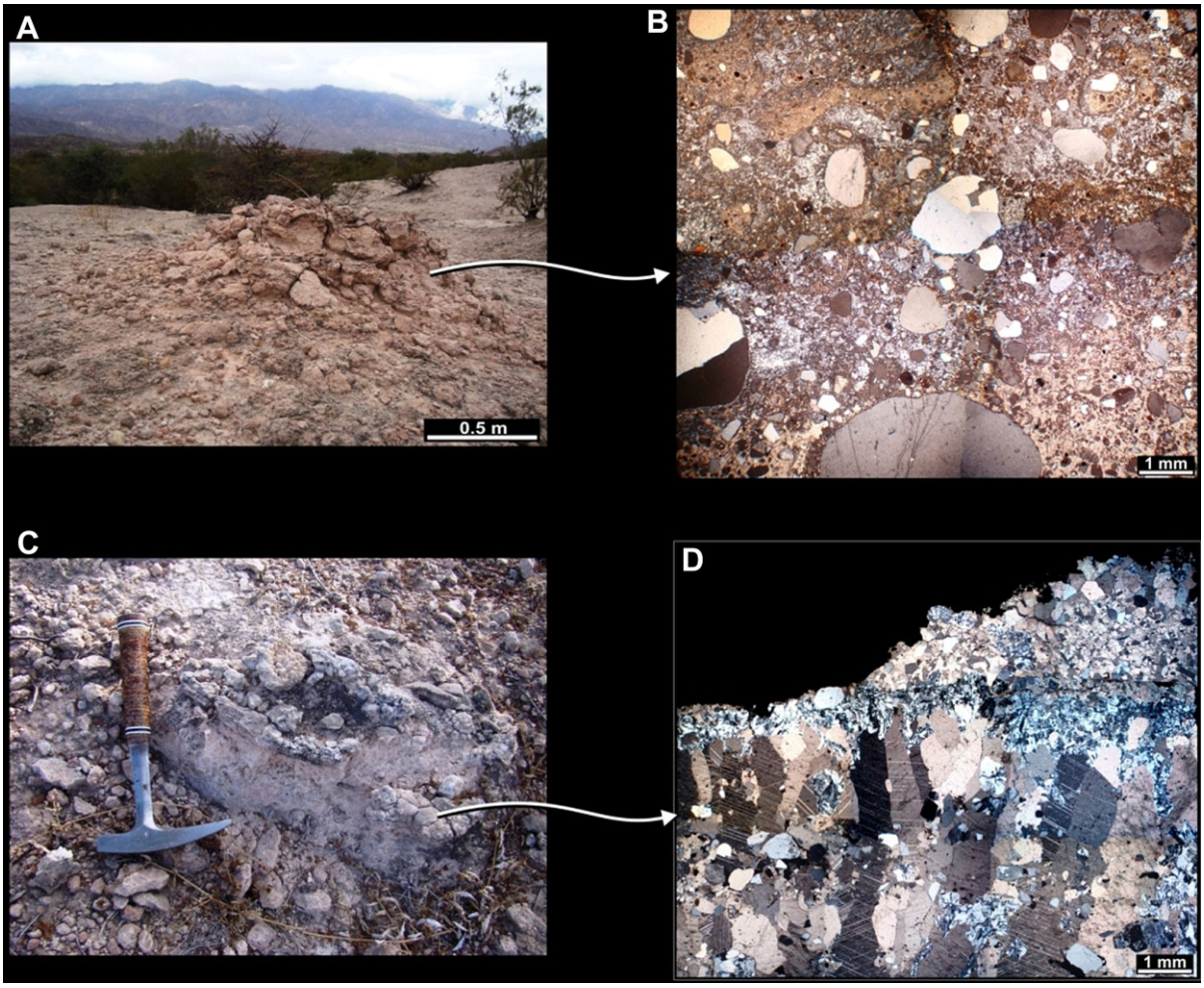

Fig. 13. Palaeohydrothermal and hot spring megastructures and microfabric from the Sangasta nesting site. A, palaeogeyser, silicified mound structure. B, thin section of the arkosic sandstone from the mound shown in A with microsilicates infilling the rock matrix. C, palaeogeyser calc-mound structure (mud-pots) with large calcite crystals at the edges. D, photomicrograph of a thin section of the calcite edge showing the internal composition and mineral phases of the "large crystalline calcite vein" with bipolar growth.

"argilization" process) replacing parts of the eggshell and egg membranes support an extreme hydrothermal eodiagenetic alteration (e.g., Deer et al., 1996; Mozita and Faure, 1998; Armbruster et al., 2006; Chardon et al., 2006; Pirajno, 2009; Mackinnon et al., 2010; Morad et al., 2010). The eggs are superficially fractured in multiple eggshell fragments (Fig. 15D, E), suggesting that the eggs were complete and not fractured at burial (Mueller-Töwe et al., 2002). Subsequently, they were exposed to extensive forces when the matrix had already at least partially solidified, thus constraining lateral extension and forcing the shells to fracture during the eodiagenesis (Grellet-Tinner and Fiorelli, 2010). The cement of the Cretaceous sandstones consists mostly of carbonate and less frequently silicate, microbialites and hydrothermal phases that originate commonly from geothermal activities, which produced the above-menioned eodiagenetic and taphonomic characteristics.

Numerous rift basins were formed from the Early Cretaceous to the Paleogene in central-western and northwestern Argentinean regions (e.g., Schmidt et al., 1995; Ramos et al., 2002; Webster et al., 2004; Chebli et al., 2005; Monaldi et al., 2008; Ramos, 2010) concomitantly to synrift basins throughout the entire South American continent (e.g., Mohriak et al., 2000; Torsvik et al., 2009; Moulin et al., 2010). Many of these rift and foreland basins are associated with the Sierras Pampeanas orogeny in central-west Argentina, which supports Bodenbender's (1911) original dating. The development of these rift basins is related in part to the opening of the South Atlantic Ocean (Schmidt et al., 1995; Ramos et al., 2002; Webster et al., 2004; Torsvik et al., 2009; Moulin et al., 2010) as well as to the back-arc subduction of the Nazca Plate below the South American Plate (Ramos, 2010), generating high regional/continental tectonism as well as volcanic activity and Cretaceous pegmatite intrusions (Comin-Chiaramonti et al., 2007; Kirstein et al., 2001; Poulsen et al., 2003). Recently, Löbens et al. (2011) presented an uplift model for the Sierras Pampeanas. According to these authors, the Sierras 2.3 km orogeny took place during the Cretaceous Period. This orogeny fostered the sedimentary basins associated with the eastern edge of the mountains and would have led to significant erosion of the pre-existing granite (about 400 m) generating the sedimentary material for basin infilling (Löbens et al., 2011; see also Webster et al., 2004). Although the Cretaceous orogeny of southeast Sierras Pampeanas ended about 80 million years ago, this process began during the Early Cretaceous (Löbens et al., 2011).

Five hydrothermal cycles, which show characteristic metallogenic and hydrothermal signatures, are recognized in association with the Sierras Pampeanas orogeny (Mutti et al., 2005a, b). These occurred during the Proterozoic, Lower–Middle Cambrian, Early–Middle Ordovician, Carboniferous–Cretaceous and Cenozoic, respectively (Mutti et al., 2005a, b). Grellet-Tinner and

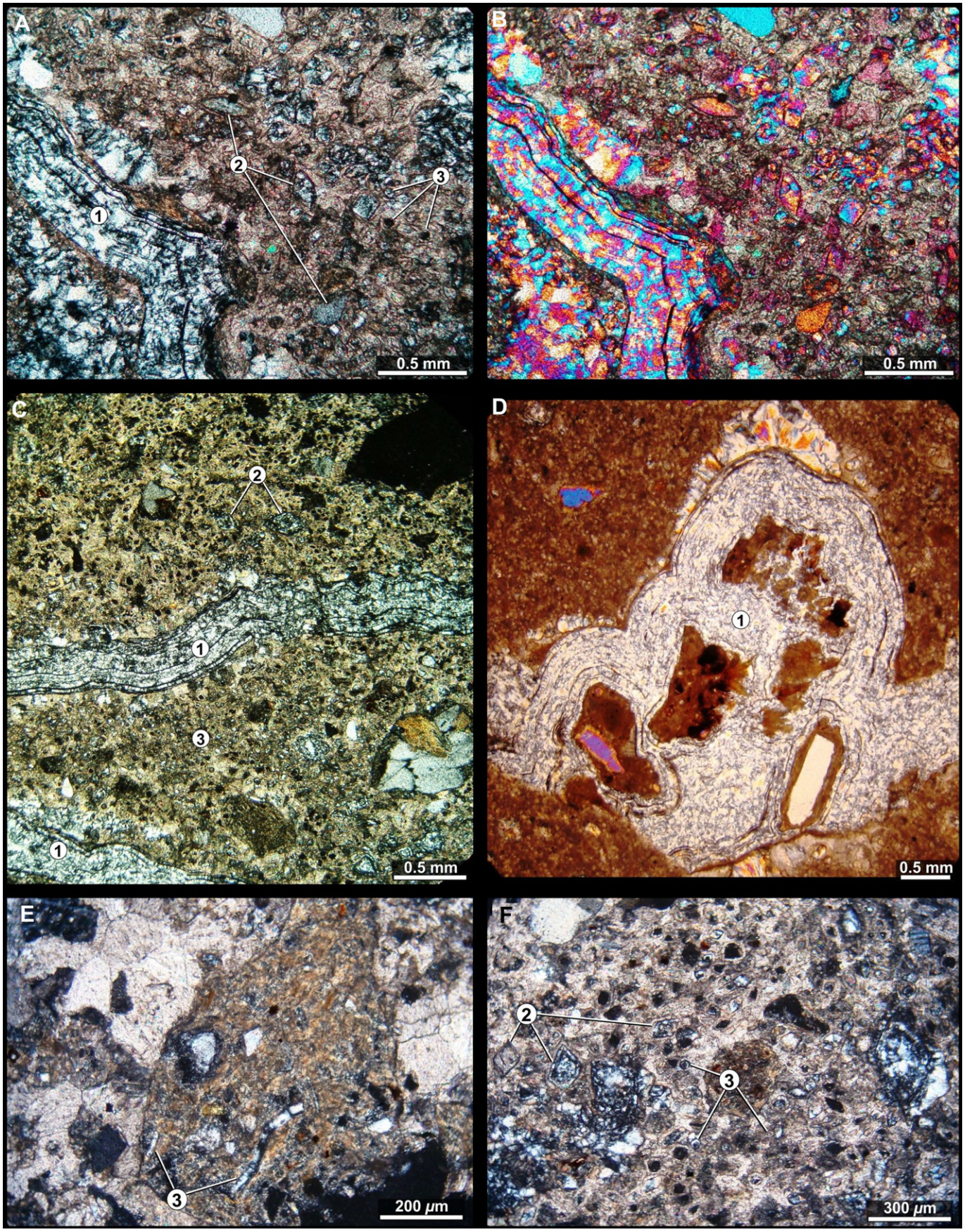
A
1
2
3
0.5 mm
B
0.5 mm
C
1
2
3
1
0.5 mm
D
1
0.5 mm
E
3
200 μm
F
2
3
300 μm

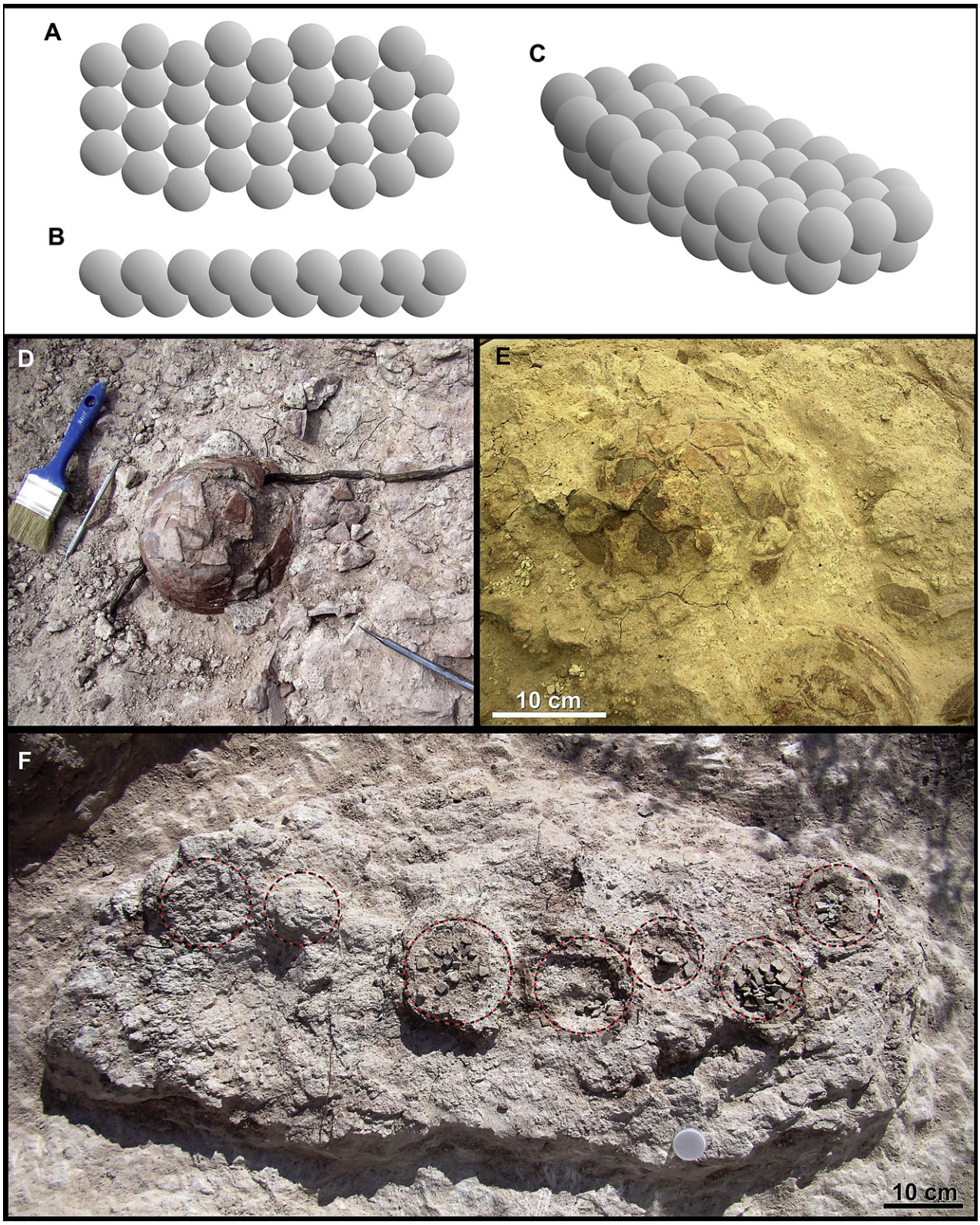

Fig. 15. Clutches and eggs from the Sanagasta nesting site. A–C, spatial arrangement of the eggs inside clutch 2 from sub-site F, one of the largest clutches at the nesting site. A, upper view. B, lateral view. C, three-dimensional view. D, complete eggs from the clutch 6 at sub-site A. E, complete eggs in clutch 2 from sub-site F. F, clutch from sub-site E (see Fig. 1) showing the spatial arrangement of seven eggs.

Fig. 14. Photomicrographs of sediments from the Sanagasta nesting site with microbialite framestones and hydrothermal microfabrics. A, B, samples from the egg-bearing sediments and lower section of Los Llanos Formation under cross nicols (A) and cross-polarized light (B). C, characteristic microbialite with long filamentous stromatoliths. D, botryoidal growth of a stromatolite. E, photomicrograph of some filaments of cyanobacteria. F, dense clustering of diatom and cyanobacteria cut crosswise; 1, 2 and 3, are stromatoliths, diatoms and cyanobacteria, respectively.

Table 2
Eggshell and sedimentary chemical analyses for the Sanagasta nesting site and Sanagasta valley.

Samples												
Oxides (weight %)	Eggshell fragments			Sediments sub-site H			Sediments sub-site F			Sediments Los Barquitos		
	Sub-site A (clutch 10)	Sub-site E (clutch 4)	Sub-site F (clutch 11)	SAN 1[b]	SAN 2[a]	SAN 6[c]	SAN 3[a]	SAN 4[a]	SAN 5[c]	SAN 7[b]	SAN 8[a]	SAN 9[c]
SiO_2	40.15	80.61	36.76	70.05	85.51	31.81	74.20	64.27	75.71	82.88	54.56	59.00
TiO_2	0.01	0.01	0.01	0.38	0.11	0.09	0.10	0.02	0.06	0.10	0.03	0.08
Al_2O_3	0.23	0.19	0.24	8.46	4.59	2.42	3.02	2.48	2.34	7.63	6.57	3.90
Fe_2O_3	0.16	0.28	0.15	2.64	1.27	0.61	1.22	0.53	0.66	1.00	0.05	0.64
MnO	0.01	0.01	0.01	0.08	0.25	0.03	0.03	0.02	0.01	0.02	0.01	0.01
MgO	0.04	0.03	0.04	0.81	0.24	0.21	0.27	0.07	0.11	0.24	0.10	0.30
CaO	32.49	7.09	30.84	1.15	1.06	35.83	9.14	15.81	8.82	0.90	17.34	16.61
Na_2O	0.06	0.06	0.06	4.56	0.90	0.36	0.30	0.52	0.47	2.28	1.24	0.73
K_2O	0.05	0.07	0.07	1.71	1.75	0.96	1.08	1.37	0.98	1.46	4.13	1.76
P_2O_5	0.01	0.02	0.02	0.07	0.04	0.18	0.09	0.05	0.04	0.03	0.04	0.04
LOI	27.77	6.59	26.77	7.82	2.90	27.54	8.82	13.08	8.20	1.90	14.43	14.30
Total	100.98	94.96	94.97	97.73	98.62	100.04	98.27	98.22	97.40	98.44	98.50	97.37
Trace elements (ppm)												
Li	<2	<2	<2	19	9	5	6	3	4	7	4	4
Ba	>2000	51	33	506	395	70	98	48	47	33	24	65
V	17	34	18	59	93	18	52	10	12	15	10	9
Cu	3	2	5	28	23	9	18	11	10	10	8	8
Zn	5	6	2	46	17	6	12	4	5	10	4	4
Pb	5	<2	<2	19	7	3	4	2	<2	<2	<2	<2
As	<5	<5	<5	11	12	10	5	<5	<5	<5	<5	<5

The lower limit for detection of the major oxides is 0.01 wt %. Limit detection for Li there is between 2 and 10,000 p.p.m.; for Ba is between 2 and 2,000 p.p.m.; for V between 1 and 10,000 p.p.m.; for Cu between 1 and 10,000 p.p.m.; for Zn between 1 and 10,000 p.p.m.; for Pb between 2 and 10,000 p.p.m.; and for As between 5 and 10,000 p.p.m.
[a] Rock sample from the lower Cretaceous levels.
[b] Rock sample from the upper Permian levels.
[c] Rock sample from the upper Cretaceous levels.

Fiorelli (2010) determined that the fourth, named the Gondwanic extensional cycle, was responsible for the geothermal activity at the Sanagasta nesting site during the Early Cretaceous. This cycle is characterized by Mn (Fe–F–Ba), F (Fe–Mn)-rich veins formed in association with granitoids and pegmatitic intrusions (Galindo et al., 1997; Rapela and Llambías, 1999; Mutti et al., 2005b). The mineralogical and geochemical characteristics of this Cretaceous cycle are the only ones that match the results of the geochemical analyses at the Sanagasta nesting site (see Mutti et al., 2005b; Grellet-Tinner and Fiorelli, 2010). This last point indicates that the egg clutches were also affected concomitantly by this Cretaceous hydrothermal process (Fig. 16), as the geochemical signature is congruent with that of the Cretaceous Gondwanic hydrothermal cycle described by Mutti et al. (2005b). This cycle includes an extensional metallogenic stage dated between the Hauterivian and Aptian (134 ± 5 and 117 ± 26 Ma; Galindo et al., 1997; Rapela and Llambías, 1999; Brodtkorb and Etcheverry, 2000; Mutti et al., 2005b), thus further delimiting the age and duration of the ovideposition and hydrothermal activities at Sanagasta (Grellet-Tinner and Fiorelli, 2010). However, and more importantly, this shows the synchronous relationship and reproductive/biological dependence of neosauropods on this specialized environment.

The E sub-site rests directly on granitoids and is characterized by only carbonate hydrothermal mineralogy. Conversely, the main nesting site exhibits, in addition to carbonates (e.g., mini-dams, terraces, mounds), bluish and grey-rimed cup-shaped (ca. 1–5 cm Ø) siliceous sinters along with plane and smooth flat sinters in close proximity to geyser and fountain mounds and clutches (Figs. 6–9). According to Schinteie et al. (2007), these silica structures are congruent with hot and hypersaturated hydrothermal solutions (Handley et al., 2005; Schinteie et al., 2007; Preston et al., 2008; Tobler et al., 2008). Moreover, irregular smaller and thin (ca. 0.5 cm Ø) cup-like siliceous sinters (Fig. 8) are interspersed regularly on the outcrop, analogous to Microfacies-4 structures in the Rotokawa geothermal field in New Zealand, which are indicative of warm (ca. 45 °C) surface and shallow-depth thermal water (Schinteie et al., 2007). However, and according to Behl (2011), small diagenetic and botryoidal opal-A microspherules reported in some eggshells (see Grellet-Tinner and Fiorelli, 2010) suggest formation temperatures below 40 °C; in addition, botryoidal silicates, domal silicified sandstone structures, and travertine veins are omnipresent at the main nesting site close to the egg-chlutches (Figs. 4F and 9F). According to Guidry and Chafetz (2003), and as fore the Yellowstone Norris Basin, the domal mounds are regarded as discharge channels with temperatures below 80 °C (Figs. 6, 7 and 9). In addition, the Lower Cretaceous levels display large calcite geodes and tubes with large scalenohedric calcite crystals with bipolar growth. According to Muchez et al. (1998), Suchy et al. (2000), Nielsen et al. (2005) and Immenhauser (2009), these crystals that generally fill cavities (Fig. 4D, E) precipitate from hot fluids at the shallow fringes of hydrothermal systems (<5 m) in low temperatures (between 30 and 50 °C) and moderately elevated salinities.

Microbialites are organosedimentary structures that result from the trapping, binding, and lithification of sediments by microbial mat communities (Burne and Moore, 1987). Thus, mineral deposits resulting from organomineralization s.l. (microbially-induced and microbially-influenced mineralization) are called microbialites (Burne and Moore, 1987; Dupraz et al., 2009) and are classified in several categories based on their macroscopic features, although they can occur as thrombolites and/or stromatolites (Burne and Moore, 1987; Riding, 1991, 2000; see Dupraz et al., 2009 for more information on calcareous microbialites). Although more common in marine sediments a few continental environments (mainly lacustrine, hypersaline and hydrothermal settings) can preserve microbial communities through biolithification (Dupraz and Visscher, 2005; Dupraz et al., 2009). The Cretaceous sedimentary level at the SGP displays several microbialite framestones formed by silicified filamentous, stratified and laminated “crust-like”

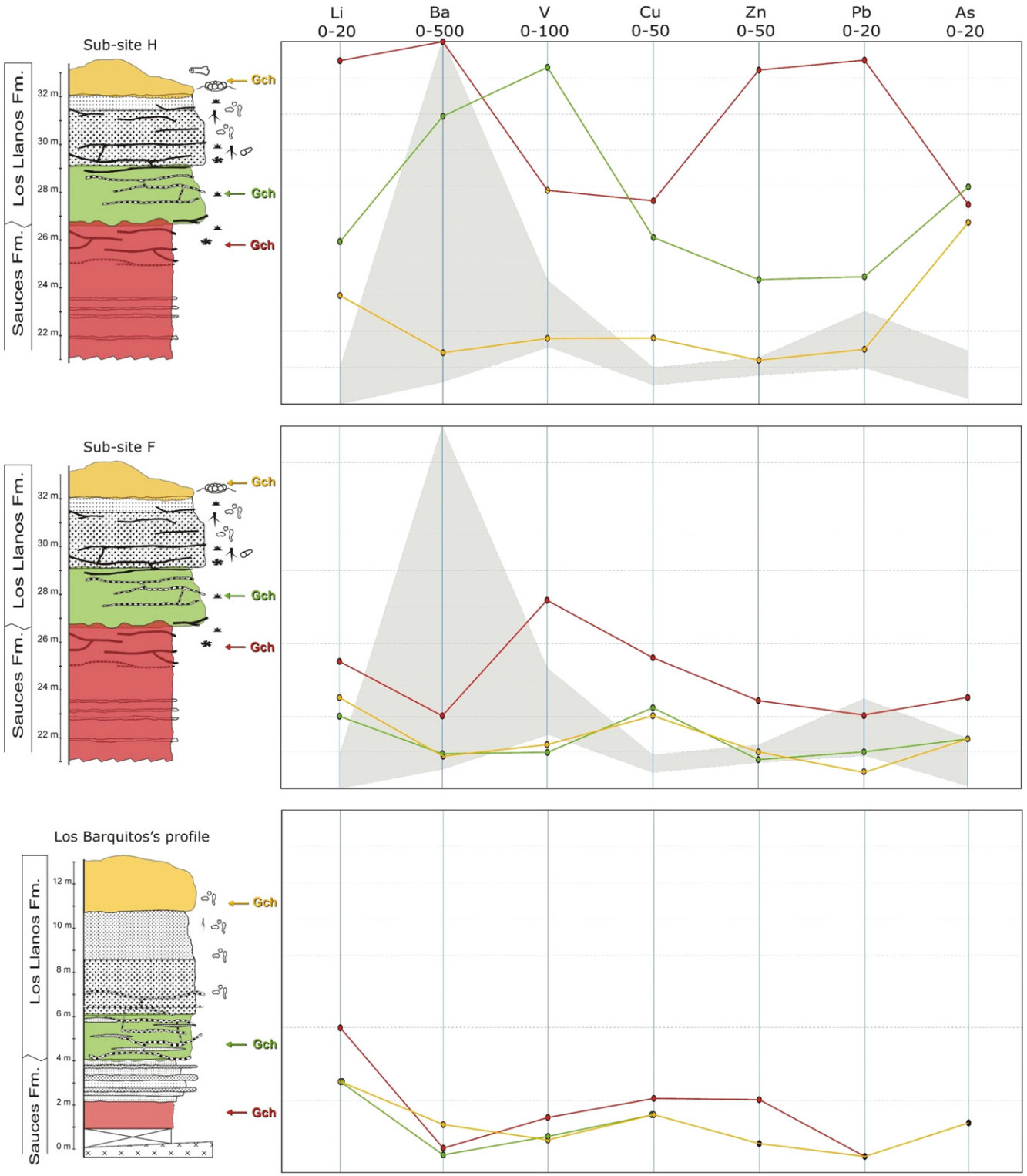

Fig. 16. Elemental analysis of the sediments and eggshell fragments from the Sanagasta nesting site and Sanagasta valley. The grey fields represent the chemical analyses of the eggshells; the red, green and yellow lines indicate the geochemical analyses of the Permian, and lower and upper egg-bearing Cretaceous sedimentary samples, respectively. (For interpretation of the references to colour in this figure legend, the reader is referred to the web version of this article.)

microstromatolits and filaments of cyanobacteria, with a dense matrix of fossil pennate diatoms (Fig. 14), which has only been reported on rare occasions from continental settings in the Cretaceous, e.g., from the Early Cretaceous Shindong Group, Gyeongsang Basin, South Korea (Harwood et al., 2004; Chang and Park, 2008). These microscopic observations confirm the presence of extremophilic (mainly thermophile and acidophile) microorganism assemblages at the nesting site, which further support the presence of a palaeohydrothermal environment.

The combined geological evidence at the SGP substantiate the presence of an epithermal palaeoenvironment (Heaney, 1993; Sillitoe, 1993; Bustillo et al., 1999; Grellet-Tinner and Fiorelli,

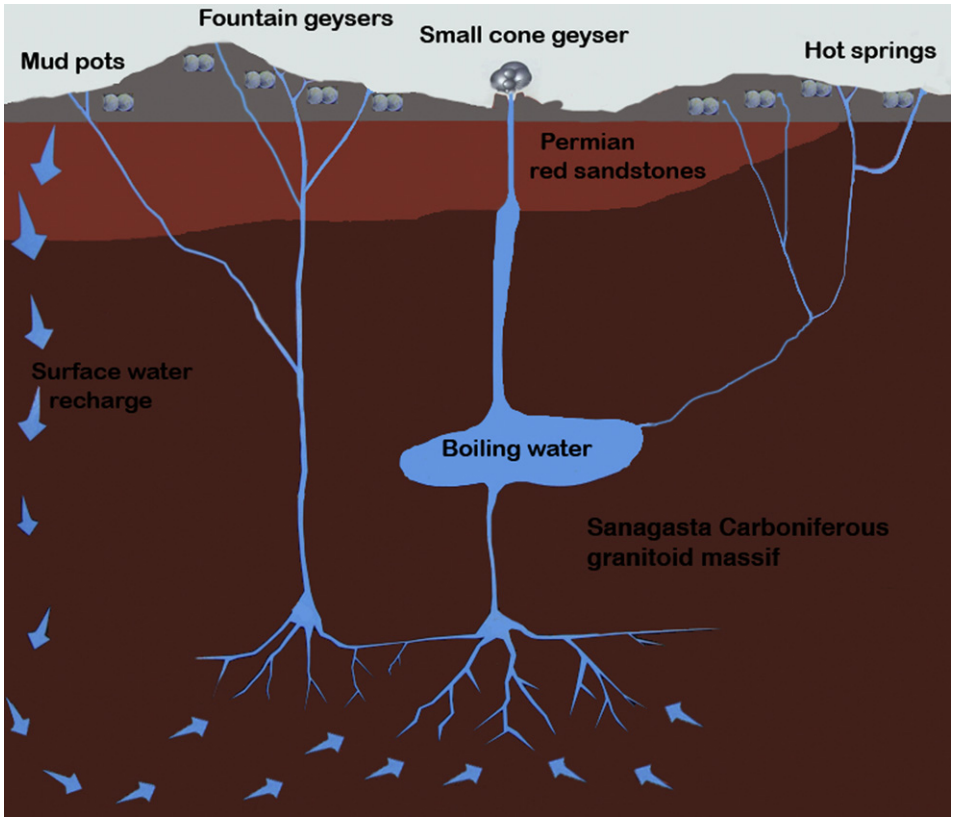

Fig. 17. Sanagasta hydrothermal environment during the Early Cretaceous.

2010) and suggest a soil temperature range from 35° to 80 °C that would have favoured the incubation of eggs 21 cm in diameter (Grellet-Tinner et al., 2012). Overall, the evidence gathered at the Sanagasta nesting site indicates that a group of neosauropods must have used geothermal soil thermoradiation and moisture to incubate their exceptionally large eggs with intricate shell strutures (Grellet-Tinner and Fiorelli, 2010; Grellet-Tinner et al., 2012). During the Early Cretaceous, the nesting site area was a localized geothermal microbasin with hot springs. It was poorly vegetated, as evidenced by the lack of silicified fossil plants, unlike that of the Jurassic geothermal ecosystems at San Agustín, Patagonia (see Channing and Edwards, 2004, 2009; Channing et al., 2007; Guido et al., 2010). As such, the area must have looked like the modern geotectonically active, Puna-like Andean landscape with hydrothermal settings like those of the El Tatio geothermal field, Antofagasta region, northern Chile (Fernandez-Turiel et al., 2005; Phoenix et al., 2006).

Recent field work at the type locality of the Los Llanos Formation and other exposures has led to the identification of numerous fossil-bearing deposits, with remains of turtles, crocodyliforms, ornithopod, sauropod and theropods ranging from fragmentary bones to semi-articulated vertebrates (Fiorelli et al., 2011), but lacking oological remains. At these localities, the Los Llanos Formation exposures are characterized by a succession of well-developed palaeosols, composed of quartz sandstones cemented by sparry calcite (calcisols). The palaeosols display paedogenetic structures (e.g., calcareous nodules, thick laminar gypsum, and abundant large rhizocretions) suggesting typical calcitic horizons interspersed by ephemeral rivers, represented by the presence of isolated fossil-bearing sandy river channels. Bioturbation, burrows, and pupal chambers (in ephemeral lake facies), and indeterminate trace fossils are also ubiquitous (Fiorelli et al., 2011).

The contrasts between these exposures of the Los Llanos Formation and the Sanagasta nesting site indicates that the latter represent a unique expression of the Early Cretaceous geothermal process that took place in the Sierras Pamepanas (see Mutti et al., 2005b) and favoured the development of a neosauropod nesting area. Similarly, the nesting sites in the Seonso Formation, South Korea (GG-T, pers obs.; Yun and Yang, 1997; Paik et al., 2004; Kim et al., 2009a) are located in the Gyeongsang Basin, which was controlled by a geotectonic setting with regional igneous activity and hydrothermal deposits (Chough et al., 2000; Choi et al., 2005a, 2005b). Although several dinosaur egg types have been reported from South Korea (see Lee, 2003), faveoloolithid types seem to be the most common (Huh and Zelenitsky, 2002; Kim et al., 2009a) in the Early–Late Cretaceous Jindong, Sihwa, and Seonso formations (Lee et al., 2001; Lee, 2003; Kim et al., 2009b). Indeed, these eggs appear usually in well-defined palaeosol levels (Paik et al., 2004) with several hydrothermal diagenetic characters (e.g., some silica structures, calcite rims and nodular calcretes). According to Paik et al. (2004), the palaeoclimate of the nesting area in the Seonso Formation was semiarid, similar to that of Sanagasta site during the Cretaceous (Fiorelli et al., 2011). Furthermore, Paik et al. (2004) suggested that the Seonso eggs were laid in excavated nests that were buried during incubation, and that the numerous clutches in several horizons is consistent with site fidelity (Paik et al., 2004). According to Choi (1986), South Korea was characterized by an Andean-type continental margin formed by subduction of the Kula Plate and was subjected to precursory extensional tectonism so that fault-bounded continental depressions developed, including the proto-Gyeongsang Basin (Choi, 1986; Lee and Lee, 2000; Hwang et al., 2008). As such, the several geological and sedimentary similarities between the dinosaur egg-bearing deposits of Gyeongsang Basin and the Los Llanos Formation, suggest that,

although separated by a considerable geographic distance different neosauropod herds adopted similar nesting behaviours with a preference for geothermal heat for egg incubation (Fig. 17).

6. Conclusion

The Cretaceous Sanagasta nesting locality represents an important breakthrough in dinosaur palaeobiology and palaeoenvironment because, for the first time, it shed lights on neosauropod reproductive biology in a specialized nesting environment, where these animals repeatedly congregated to ovideposit their eggs. The present paper describes in detail the geology and sedimentology in order to assess the palaeoenvironment of this specialized nesting site. The geochemical analyses results and microscopic observations on the sedimentary microstructure, microfacies, and microfabric reveal the epithermal features of the nesting site and adaptative biological interdependencies in this unusual geological setting. Moreover, our study offers a partial answer to the general question as to why neosauropod nesting sites were confined to a few selected localities during the Cretaceous Period. Equally importantly, the results of our research at Sanagasta provide new and valuable information on regional geology and resolve the longstanding debate about the relative age of the Sierras Pampeanas Orientales sedimentary basins. The age of the Los Llanos Formation has been the topic of long and controversial debates. Now, an Early Cretaceous age (Hauterivian–Aptian, ca. 134–117 million years) can be confidently assigned to this formation; in addition, the well-developed palaeo-calcisols recently discovered associated with fossil assemblage in other exposures without nests in the Los Llanos Formation confirm this age determination.

The Sanagasta site is not the only one to reveal an adaptive and reproductive biological interdependence of neosauropod dinosaurs to geothermal environments. The faveoloolithid nesting sites in the Early–Late Cretaceous Jindong, Sihwa, and Seonso formations in South Korea are also located in basins controlled by geotectonic settings and dominated by hydrothermal activity. This region was also characterized by an Andean-type continental margin. The geological and oological similarities between the Sanagasta and Seonso nesting sites suggest that the choice of geothermal localities for ovideposition by neosauropods was perhaps not a random or isolated event in the Early Cretaceous and, therefore, possibly implies a recurrent symbiotic relationship with geothermal localities for nesting purposes by this dinosaur clade.

Acknowledgements

We acknowledge the help of CRILAR staff and particularly the CRILAR technicians: Sergio de la Vega, Roxana Brizuela and Carlos A. Bustamante. We thank to Mariano Larrovere, Jean Le Loeuff, Sebastian Apesteguía, Ivana Amelotti, Eloisa Argañaraz, Ricardo Astini, Laura Chornogubsky, Laura Cruz, Maru Fernandez, Ann Göth, Alejandro Kramarz, Teresa Manera de Bianco, Diego Pol, Pablo Puerta, Rubén D. Juárez Vallieri, José Carballido, Jimmy Powell, Leonardo Salgado, Edith Simón, Martín Zpiola, and Rodrigo Tomassini, for their continuous support, comments, and access to fossil egg material under their care and Tec. F. Tricarico (MACN) and Biol. E. Crestpo (UNSL) for their help with the SEM microscope. We acknowledge Ricardo Astini, Teresa Sánchez, Marcelo Carrera and Emilio Vaccari for their help and also thank the two anonymous referees for their comments and valuable suggestions. We are thankful to David Batten for his help editing our manuscript. We are grateful to Beba de Soria, Secretaría de Cultura La Rioja, Arq. Valeria Soriano and Gobierno de La Rioja for their financial support. LF, GGT and EA also thank Dra. Teresa Sánchez (CIPAL) for her valuable support. Our study was made possible with funding from the Secretaría de Cultura de La Rioja and the Consejo Federal de Ciencia y Tecnología (COFECYT) (SCTIP N°1198/06 – Proyecto LR02/06). GGT would like to acknowledge particularly Gobierno de La Rioja, Luis Beder Herrera and Valeria Soriano for supporting his travel and research in La Rioja Province.

References

Adams, A.E., MacKenzie, W.S., 1998. A color atlas of carbonate sediments and rocks under the microscope. Mason Wiley, England, 180 pp.

Arenas-Abad, C., Vázquez-Urbez, M., Pardo-Tirapu, G., Sancho-Marcén, C., 2010. Fluvial and associated carbonate deposits. In: Alonso-Zarza, A.M., Tanner, L.H. (Eds.), Carbonates in Continental Settings: Facies, Environments, and Processes. Developments in Sedimentology 61, Elsevier, Amsterdam, pp. 133–175.

Arcucci, A.B., Marsicano, C.A., Caselli, A.T., 2004. Tetrapod association and palaeoenvironment of the Los Colorados Formation (Argentina): a significant sample from Western Gondwana at the end of the Triassic. Geobios 37, 557–568.

Arcucci, A.B., Marsicano, C.A., Coria, R.A., 2005. Una nueva localidad fosilífera en el Cretácico de la Precordillera de La Rioja. Ameghiniana 42 (4, Supplement), 60R.

Armbruster, T., Bonazzi, P., Akasaka, M., Bermanec, V., Chopin, C., Gieré, R., Heuss-Assbichler, S., Liebscher, A., Menchetti, S., Pan, Y., Pasero, M., 2006. Recommended nomenclature of epidote-group minerals. European Journal of Mineralogy 18, 551–567.

Benning, L.G., Phoenix, V.R., Mountain, B.W., 2005. Biosilicification: the role of cyanobacteria in silica sinter deposition. In: Gadd, G.M., Semple, K.T., Lappin-Scott, H.M. (Eds.), Micro-organisms and Earth Systems – Advances in Geomicrobiology. Cambridge University Press, Cambridge, pp. 131–150.

Behl, R.J., 2011. Chert spheroids of the Monterey Formation, California (USA): early-diagenetic structures of bedded siliceous deposits. Sedimentology 58, 325–351.

Bodenbender, G., 1911. Constitución Geológica de la parte meridional de La Rioja y regiones limítrofes, R. Argentina. Boletín de la Academia Nacional de Ciencias 19 (1), 5–221.

Boggs, S., Jr., 1992. Petrology of Sedimentary Rocks. Merrill/Macmillan, London, 707 pp.

Bonaparte, J.F., 1978. El Mesozoico de América del Sur y sus tetrápodos. Opera Lilloana 26, 596 pp.

Bonaparte, J.F., 1997. El Triásico de San Juan – La Rioja Argentina y sus Dinosaurios. Museo Argentino de Ciencias Naturales, 190 pp.

Bordas, A.F., 1941. Nuevos restos fósiles de la Formación de Los Llanos (San Luis). Physis 19, 23–27.

Brodtkorb, M.K., Etcheverry, R., 2000. Edad K/Ar de la mineralización de manganeso de Aguada del Monte, provincia de Córdoba. Revista de la Asociación Geológica Argentina 55, 280–283.

Browne, P.R.L., 1991. Mineralogical guides to interpreting the shallow paleohydrology of epithermal mineral depositing environments. In: Freeston, D.H., Browne, P.R.L., Scott, G.L. (Eds.), Proceedings of the 13th New Zealand Geothermal Workshop, Auckland, New Zealand. Geothermal Institute, University of Auckland, pp. 263–269.

Burne, R.V., Moore, L.S., 1987. Microbialites: organosedimentary deposits of benthic microbial communities. Palaios 2, 241–254.

Bustillo, M.A., Garcia-Guinea, J., Martinez-Frias, J., Delgado, A., 1999. Unusual sedimentary geodes filled by gold-bearing hematite laths. Geological Magazine 136, 671–679.

Cady, S.L., Farmer, J.D., 1996. Fossilization processes in siliceous thermal springs: trends in preservation along thermal gradients. In: Brock, G.P., Goode, J.A. (Eds.), Evolution of Hydrothermal Ecosystems on Earth (and Mars?). John Wiley, Chichester, pp. 150–173.

Campbell, K.A., Rodgers, K.A., Brotheridge, J.M.A., Browne, P.R.L., 2002. An unusual modern silica–carbonate sinter from Pavlova spring, Ngatamariki, New Zealand. Sedimentology 49, 835–854.

Carroll, S., Mroczek, E., Alai, M., Ebert, M., 1998. Amorphous silica precipitation (60 to 120 °C): comparison of laboratory and field rates. Geochimica et Cosmochimica Acta 62, 1379–1396.

Casadío, S., Manera, T., Parras, A., Montalvo, C.I., 2002. Huevos de dinosaurios (Faveoloolithidae) del Cretácico Superior de la cuenca del Colorado, provincia de La Pampa, Argentina. Ameghiniana 39, 285–293.

Chang, K.H., Park, S.O., 2008. Early Cretaceous tectonism and diatoms in Korea. Acta Geologica Sinica 82, 1179–1184.

Channing, A., Edwards, D., 2004. Experimental taphonomy: silicification of plants in Yellowstone hot spring environments. Transactions of the Royal Society of Edinburgh: Earth Sciences 94, 503–521.

Channing, A., Edwards, D., 2009. Silicification of higher plants in geothermally influenced wetlands: Yellowstone as a Lower Devonian Rhynie analog. Palaios 24, 505–521.

Channing, A., Zamuner, A.B., Zúñiga, A., 2007. A new Middle–Late Jurassic flora and hot spring chert deposit from the Deseado Massif, Santa Cruz province, Argentina. Geological Magazine 144, 401–411.

Chardon, E.E., Livens, F.R., Vaughan, D.J., 2006. Reactions of feldspar surfaces with aqueous solutions. Earth-Science Reviews 78, 1–26.

Chebli, G.A., Spalletti, L., Rivarola, E., De Elorriaga, E., Webster, R., 2005. Cuencas Cretácicas de la Región Central. In: Chebli, G., Cortiñas, J., Spalletti, L., Legarreta, L., Vallejo, E. (Eds.), Simposio Frontera Exploratoria de la Argentina, VI Congreso de Exploración y Desarrollo de Hidrocarburos, Mar del Plata, pp. 193–215.

Choi, H.I., 1986. Sedimentation and evolution of the Cretaceous Gyeongsang Basin, southeastern Korea. Journal of the Geological Society 143, 29–40.
Choi, S.G., Kwon, S.T., Ree, J.H., So, C.S., Pak, S.J., 2005a. Origin of Mesozoic gold mineralization in South Korea. The Island Arc 14, 102–114.
Choi, S.G., Ryu, I.C., Pak, S.J., Wee, S.M., Kim, C.S., Park, M.E., 2005b. Cretaceous epithermal gold-silvermineralization and geodynamic environment, Korea. Ore Geology Review 26, 115–135.
Choquette, P.W., Pray, L.C., 1970. Geologic nomenclature and classification of porosity in sedimentary carbonates. American Association of Petroleum Geologists, Bulletin 54, 207–250.
Chough, S.K., Kwon, S.-T., Ree, J.-H., Choi, D.K., 2000. Tectonic and sedimentary evolution of the Korean peninsula: a review and new view. Earth-Science Reviews 52, 175–235.
Ciccioli, P.L., Ballent, S., Tedesco, A.M., Barreda, V., Limarino, C.O., 2005. Hallazgo de depósitos cretácicos en la Precordillera de La Rioja (Formación Cienága del Río Huaco). Revista de la Asociación Geológica Argentina 60, 385–394.
Comin-Chiaramonti, P., Marzoli, A., Barros Gomes, C., Milan, A., Riccomini, C., Fernandez Velázquez, V., Mantovani, M.M.S., Renne, P., Gaeta Tassinari, C.C., Vasconcelos, P.M., 2007. The origin of post-Paleozoic magmatism in the eastern Paraguay. Geological Society of America, Special Paper 430, 603–633.
Dávila, F.M., Astini, R.A., Jordan, T.E., Gehrels, G., Ezpeleta, M., 2007. Miocene fore-bulge development previous to broken foreland partitioning in the southern Central Andes, west-central Argentina. Tectonics 16, TC5016.
de Valais, S., Apesteguía, S., Udrizar Sauthier, D., 2003. Nuevas evidencias de dinosaurios de la Formación Puerto Yeruá (Cretácico), Provincia de Entre Ríos, Argentina. Ameghiniana 40, 631–635.
Deer, W.W., Howie, R.A., Zussman, J., 1996. An Introduction to the Rock-forming Minerals. Prentice Hall/Pearson, Harlow, 712 pp.
Dunham, R.J., 1962. Classification of carbonate rocks according to their depositional texture. In: Ham, W.E. (Ed.), Classification of Carbonate Rocks – a symposium. American Association of Petroleum Geologists, Memoir 1, pp. 108–121.
Dupraz, C., Reid, R.P., Braissant, O., Decho, A.W., Norman, R.S., Visscher, P.T., 2009. Processes of carbonate precipitation in modern microbial mats. Earth-Science Reviews 96, 141–162.
Dupraz, C., Visscher, P.T., 2005. Microbial lithification in marine stromatolites and hypersaline mats. Trends in Microbiology 13, 429–438.
Ezpeleta, M., Dávila, F.M., Astini, R.A., 2006. Estratigrafía y paleoambientes de la Formación Los Llanos (La Rioja): una secuencia condensada miocena en el antepaís fragmentado andino central. Revista de la Asociación Geológica Argentina 61, 171–186.
Fernandez-Turiel, J.L., Garcia-Valles, M., Gimeno-Torrente, D., Saavedra-Alonso, J., Martinez-Manent, S., 2005. The hot spring and geyser sinters of El Tatio, northern Chile. Sedimentary Geology 180, 125–147.
Fiorelli, L.E., Grellet-Tinner, G., Argañaraz, E., Larrovere, M.A., Chornogubsky, L., Torrens, J., Hechenleitner, M., 2011. Record of the first Cretaceous continental fauna from La Rioja Province, northwestern Argentina: geo-paleontological implications. Latinamerika-Kolloquium 2011, Heidelberg, Germany, Abstracts and Program, p. 83.
Flügel, E., 2010. Microfacies of Carbonate Rocks: Analysis, Interpretation and Application. Springer-Verlag, Berlin, 984 pp.
Folk, R.L., 1962. Spectral subdivision of limestone types. In: Ham, W.E. (Ed.), Classification of Carbonate Rocks–a symposium. American Association of Petroleum Geologists, Memoir 1, pp. 62–84.
Fouke, B.W., Bonheyo, G.T., Sanzenbacher, B., Frías-López, J., 2003. Partitioning of bacterial communities between travertine depositional facies at Mammoth Hot Springs, Yellowstone National Park, U.S.A. Canadian Journal of Earth Sciences 40, 1531–1548.
Galindo, C., Pankhurst, R., Casquet, C., Coniglio, J., Baldo, E., Rapela, C., Saavedra, J., 1997. Age, Sr- and Nd-isotope systematics, and origin of two fluorite lodes, Sierras Pampeanas, Argentina. International Geology Review 39, 948–954.
Grellet-Tinner, G., Fiorelli, L.E., 2010. A new Argentinean nesting site showing neosauropod dinosaur reproduction in a Cretaceous hydrothermal environment. Nature Communications 1, 32, doi:10.1038/ncomms1031.
Grellet-Tinner, G., Fiorelli, L.E., Salvador, R.B., 2012. Water vapor conductance of the Lower Cretaceous dinosaur eggs from Sanagasta, La Rioja, Argentina – paleobiological and paleoecological implications for South American faveoloolithid and megaloolithid eggs. Palaios 27, doi:10.2110/palo.2011.p11-061r.
Grellet-Tinner, G., Sim, C.M., Kim, D.H., Trimby, P., Higa, A., An, S.L., Oh, H.S., Kim, T.J., Kardjilov, N., 2011. Description of the first lithostrotian titanosaur embryo in ovo with neutron characterization and implications for lithostrotian Aptian migration and dispersion. Gondwana Research 20, 621–629.
Grosse, P., Söllner, F., Baéz, M.A., Toselli, A.J., Rossi, J.N., de la Rosa, J.D., 2009. Lower Carboniferous post-orogenic granites in central-eastern Sierra de Velasco, Sierras Pampeanas, Argentina: U–Pb monazite geochronology, geochemistry and Sr–Nd isotopes. International Journal of Earth Sciences 98, 1001–1025.
Guido, D.M., Channing, A., Campbell, K.A., Zamuner, A., 2010. Jurassic geothermal landscapes and ecosystems at San Agustín, Patagonia, Argentina. Journal of the Geological Society, London 167, 11–20.
Guidry, S.A., Chafetz, H.S., 2002. Factors governing subaqueous siliceous sinter precipitation in hot springs: examples from Yellowstone National Park, USA. Sedimentology 49, 1253–1267.
Guidry, S.A., Chafetz, H.S., 2003. Anatomy of siliceous hot springs: examples from Yellowstone National Park, Wyoming, USA. Sedimentary Geology 157, 71–106.
Guiñazú, J.R., 1962. Los llamados "Estratos de Los Llanos" en la Provincia de San Luis y su contenido de rodados de rocas andesíticas y restos de mamíferos fósiles. Anales de las Primeras Jornadas Geológicas Argentinas 2, 89–95.
Handley, K.M., Campbell, K.A., Mountain, B.W., Browne, P.R.L., 2005. Abiotic-biotic controls on the origin and development of spicular sinter: in situ growth experiments, Champagne Pool, Waiotapu, New Zealand. Geobiology 3, 93–114.
Harwood, D.M., Chang, K.H., Nikolaev, V.A., 2004. Late Jurassic to earliest Cretaceous diatoms from Jasong Synthem, southern Korea: evidence for a terrestrial origin. In: Witkowski, A., Radziejewska, T., Wawrzyniak-Wydrowska, B., Daniszewska-Kowalczyk, G., Bak, M. (Eds.), Abstracts, 18th International Diatom Symposium, Miedzyzdroje, Poland, p. 81.
Heaney, P.J., 1993. A proposed mechanism for the growth of chalcedony. Contributions to Mineralogy and Petrology 15, 66–74.
Huh, M., Zelenitsky, D.K., 2002. Rich dinosaur nesting site from the Cretaceous of Bosung County, Chullanam-Do Province, South Korea. Journal of Vertebrate Paleontology 22, 716–718.
Hwang, B.H., Son, M., Yang, K., Yoon, J., Ernst, W.G., 2008. Tectonic evolution of the Gyeongsang Basin, southeastern Korea from 140 Ma to the Present, based on a strike-slip and block rotation tectonic model. International Geology Review 50, 343–363.
Immenhauser, A., 2009. Phreatic cave calcites – archives of two realms. Geology Today 25, 29–33.
Jones, B., Renaut, R.W., Rosen, M.R., Klyen, L., 1998. Primary siliceous rhizoliths from Loop Road hot springs, North Island, New Zealand. Journal of Sedimentary Research 68, 115–123.
Kim, C.-B., Al-Aasm, I.S., Ghazban, F., Chang, H.-W., 2009a. Stable isotopic composition of dinosaur eggshells and pedogenic carbonates in the Upper Cretaceous Seonso Formation, South Korea: paleoenvironmental and diagenetic implications. Cretaceous Research 30, 93–99.
Kim, S.B., Kim, Y.G., Jo, H.R., Jeong, K.S., Chough, S.K., 2009b. Depositional facies, architecture and environments of the Sihwa Formation (Lower Cretaceous), mid-west Korea with special reference to dinosaur eggs. Cretaceous Research 30, 100–126.
Kirstein, L.A., Kelley, S., Hawkesworth, C., Turner, S., Mantovani, M., Wijbrans, J., 2001. Protracted felsic magmatic activity associated with the opening of the South Atlantic. Journal of the Geological Society, London 158, 583–592.
Konhauser, K.O., Jones, B., Reysenbach, A.L., Renaut, R.W., 2003. Hot spring sinters: keys to understanding Earth's earliest life forms. Canadian Journal of Earth Sciences 40, 1713–1724.
Konhauser, K.O., Phoenix, V.R., Lalonde, S.V., 2008. Bacterial biomineralization: Where to from here? Geobiology 6, 298–302.
Lee, J.I., Lee, Y.I., 2000. Provenance of the Lower Cretaceous Hayang Group, Gyeongsang Basin, southeastern Korea: implications for continental-arc volcanism. Journal of Sedimentary Research 70, 151–158.
Lee, Y.N., 2003. Dinosaur bones and eggs in South Korea. Memoir of the Fukui Prefectural Dinosaur Museum 2, 113–121.
Lee, Y.N., Yu, K.M., Word, C.B., 2001. A review of vertebrate faunas from the Gyeongsang Supergroup (Cretaceous) in South Korea. Palaeogeography, Palaeoclimatology, Palaeoecology 165, 357–373.
Limarino, O., Poma, S., 1999. Hoja Geológica Chamical, 3166 – I. Provincias de La Rioja, San Luis y San Juan, Programa Nacional de Cartas Geológicas. Convenio SEGEMAR – UBA., 35 pp.
Löbens, S., Bense, F.J., Wemmer, K., Dunkl, I., Costa, C.H., Layer, P., Siegesmund, S., 2011. Exhumation and uplift of the Sierras Pampeanas: preliminary implications from K–Ar fault gouge dating and low-T thermochronology in the Sierra de Comechingones (Argentina). International Journal of Earth Science 100, 671–694.
Mackinnon, I.D.R., Millar, G.J., Stolz, W., 2010. Low temperature synthesis of zeolite N from kaolinites and montmorillonites. Applied Clay Science 48, 622–630.
Margulis, L., 1998. Symbiotic Planet: A New Look at Evolution. Basic Books, New York, NY, 176 pp.
Melchor, R.N., de Valais, S., Genise, J.F., 2002. The oldest bird-like fossil footprints. Nature 417, 936–938.
Mohriak, W.U., Bassetto, M., Vieira, I.S., 2000. Tectonic evolution of the rift basins in the northeastern Brazilian region. In: Mohriak, W., Talwani, M. (Eds.), Atlantic Rifts and Continental Margins. Geophysics Monograph 115, pp. 293–315.
Monaldi, C.R., Salfity, J.A., Kley, J., 2008. Preserved extensional structures in an inverted Cretaceous rift basin, northwestern Argentina: outcrop examples and implications for fault reactivation. Tectonics 27, TC1011, doi:10.1029/2006TC001993.
Morad, S., El-Ghali, M.A.K., Caja, M.A., Sirat, M., Al-Ramadan, K., Mansurbeg, H., 2010. Hydrothermal alteration of plagioclase in granitic rocks from Proterozoic basement of SE Sweden. Geological Journal 45, 105–116.
Moulin, M., Aslanian, D., Unternehr, P., 2010. A new starting point for the South and Equatorial Atlantic Ocean. Earth-Science Reviews 98, 1–37.
Mozita, C., Faure, K., 1998. Hydrothermal origin of smectite in volcanic ash. Clays and Clays Minerals 46, 178–182.
Muchez, P., Nielsen, P., Sintubin, M., Lagrou, D., 1998. Conditions of meteoric calcite formation along a Variscan fault and their possible relation to climatic evolution during the Jurassic-Cretaceous. Sedimentology 45, 845–854.
Mueller-Töwe, I.J., Sander, P.M., Schuller, H., Thies, D., 2002. Hatching and infilling of dinosaur eggs as by computed tomography. Palaeontographica Abteilung A 267, 119–168.
Mutti, D., Di Marco, A., Tourn, S., Herrmann, C., Geuna, S., Caccaglio, O., González Chiozza, S., 2005a. Evolución metalogenética de las Sierras Pampeanas de Córdoba y sur de Santiago del Estero, Argentina: ciclos Prepampeano y Pampeano. Revista de la Asociación Geológica Argentina 60, 104–121.

Mutti, D., Tourn, S., Caccaglio, O., Herrmann, C., Geuna, S., Di Marco, A., González Chiozza, S., 2005b. Evolución metalogenética de las Sierras Pampeanas de Córdoba y sur de Santiago del Estero: ciclos famatiniano, gondwánico y ándico. Revista de la Asociación Geológica Argentina 60, 467–485.

Nielsen, P., Muchez, P., Heijlen, W., Fallick, A.E.T., Keppens, E., Weis, D., Swennen, R., 2005. Columnar calcites as testimony of diagenetic overprinting at the boundary between Upper Tournaisian dolomites and limestones (Belgium): multiple origins for apparently similar features. Sedimentology 52, 945–967.

Owen, R.A., Owen, R.B., Renaut, R.W., Scott, J.J., Jones, B., Ashley, G.M., 2008. Mineralogy and origin of rhizoliths on the margins of saline, alkaline Lake Bogoria, Kenya Rift Valley. Sedimentary Geology 203, 143–163.

Paik, I.S., Huh, M., Kim, H.J., 2004. Dinosaur egg-bearing deposits (Upper Cretaceous) of Boseong, Korea: occurrence, palaeoenvironments, taphonomy, and preservation. Palaeogeography, Palaeoclimatology, Palaeoecology 205, 155–168.

Pascual, R., 1954. Adiciones a la fauna de la Formación de Los Llanos de San Luis y su edad. Revista del Museo Municipal de Ciencias Naturales y Tradición de Mar del Plata 1, 113–121.

Pentecost, A., 2005. Travertine. Springer-Verlag, Berlin, 446 pp.

Pentecost, A., Renaut, R.W., Jones, B., 2003. What is a Hot spring? Journal of Earth Science 40, 1443–1446.

Pettijohn, F.J., Potter, P.E., Siever, R., 1987. Sand and Sandstone, second ed. Springer-Verlag, Berlin, 553 pp.

Phoenix, V.R., Bennett, P.C., Engel, A.S., Tyler, S.W., Ferris, F.G., 2006. Chilean high-altitude hot-spring sinters: a model system for UV screening mechanisms by early Precambrian cyanobacteria. Geobiology 4, 15–28.

Pieroni, E.M., Georgieff, E.M., 2007. Reconsideración estratigráfica del Neopaleozoico de los alrededores del dique Los Sauces, La Rioja. Revista de la Asociación Geológica Argentina 62, 105–115.

Pirajno, F., 2009. Hydrothermal Processes and Mineral Systems. Springer-Verlag, Berlin, 250 pp.

Poulsen, C.J., Gendaszek, A.S., Jacob, R.L., 2003. Did the rifting of the Atlantic Ocean cause the Cretaceous thermal maximum? Geology 31, 115–118.

Preston, L.J., Benedix, G.K., Genge, M.J., Sephton, M.A., 2008. A multidisciplinary study of siliceous sinter deposits with applications to silica identification and detection of fossil life on Mars. Icarus 198, 331–350.

Ramos, V.A., 2010. The tectonic regime along the Andes: present-day and Mesozoic regimes. Geological Journal 45, 2–25.

Ramos, V.A., Cristallini, E.O., Pérez, D.J., 2002. The Pampean flat-slab of the Central Andes. Journal of South American Earth Sciences 15, 59–78.

Rapela, C.W., Llambías, E.J., 1999. El magmatismo Gondwánico y los ciclos Fanerozoicos. In: Caminos, R. (Ed.), Geología Argentina, SEGEMAR, Anales 29 (14: 3), pp. 373–376.

Renaut, R.W., Jones, B., 2003. Sedimentology of hot spring systems. Canadian Journal of Earth Sciences 40, 1439–1442.

Reysenbach, A.L., Cady, S.L., 2001. Microbiology of ancient and modern hydrothermal systems. Trends in Microbiology 9, 79–86.

Riding, R., 1991. Classification of microbial carbonates. In: Riding, R. (Ed.), Calcareous Algae and Stromatolites. Springer-Verlag, New York, pp. 21–51.

Riding, R., 2000. Microbial carbonates: the geological record of calcified bacterial-algal mats and biofilms. Sedimentology 47 (Supplement 1), 179–214.

Rogers, R.R., Arcucci, A.B., Abdala, F., Sereno, P.C., Forster, C.A., May, C.L., 2001. Paleoenvironment and taphonomy of the Chañares Formation tetrapod assemblage (Middle Triassic), northwestern Argentina: spectacular preservation in volcanogenic concretions. Palaios 16, 461–481.

Rothschild, L.J., Mancinelli, R.L., 2001. Life in extreme environments. Nature 409, 1092–1101.

Rusconi, C., 1936. Restos de mamíferos terciarios de San Luis. Boletín Paleontológico Buenos Aires 6, 1–14.

Ruskin, B.G., 2006. Sequence stratigraphy and paleopedology of nonmarine foreland basins: Iglesia Basin, Argentina and Axhandle Basin, Utah. Unpublished PhD dissertation, Cornell University, Ithaca, NY, 511 pp.

Ruskin, B.G., Dávila, F.M., Hoke, G.D., Jordan, T.E., Astini, R.A., Alonso, R., 2011. Stable isotope composition of middle Miocene carbonates of the Frontal Cordillera and Sierras Pampeanas: Did the Paranaense seaway flood western and central Argentina? Palaeogeography, Palaeoclimatology, Palaeoecology 308, 293–303.

Schinteie, R., Campbell, K.A., Browne, P.R.L., 2007. Microfacies of stromatolitic sinter from acid-sulphate chloride springs at Parariki Stream, Rotokawa Geothermal Field, New Zealand. Palaeontologia Electronica 10, 4A, 33 pp.

Schmidt, C.J., Astini, R.A., Costa, C.H., Gardini, C.E., Kraemer, P.E., 1995. Cretaceous rifting, alluvial fan sedimentation and Neogene invertion, southern Sierras Pampeanas, Argentina. In: Tankard, A.J., Suárez Soruco, R., Welsink, H.J. (Eds.), Petroleum Basins of South America. American Association of Petroleum Geologists, Memoir 62, pp. 341–358.

Scholle, P.A., Ulmer-Scholle, D.S., 2003. A color guide to the petrography of carbonate rocks: grains, textures, porosity, diagenesis. American Association of Petroleum Geologists, Memoir 77, 470 pp.

Sillitoe, R.H., 1993. Epithermal models: genetic types, geometric controls and shallow features. In: Kirkham, R.V., Sinclair, W.D., Thorpe, R.I., Duke, J.M. (Eds.), Mineral Deposit Modeling. Geological Association of Canada, Special Volume 40, pp. 403–417.

Simón, M.E., 2006. Cáscaras de huevos de dinosaurios de la Formación Allen (Campaniano–Maastrichtiano), en Salitral Moreno, provincia de Río Negro, Argentina. Ameghiniana 43, 513–528.

Suchy, V., Heijlen, W., Sykorova, I., Muchez, P., Dobes, P., Hladikova, J., Jackova, J., Safanda, J., Zeman, A., 2000. Geochemical study of calcite veins in the Silurian and Devonian of the Barrandian Basin (Czech Republic): evidence for widespread post-Variscan fluid flow in the central part of the Bohemian Massif. Sedimentary Geology 131, 201–219.

Tauber, A.A., 2007. Primer yacimiento de huevos de dinosaurios (Cretácico Superior) de la provincia de La Rioja, Argentina. Ameghiniana 44, 11–28.

Tedesco, A.M., Limarino, C.O., Ciccioli, P.L., 2007. Primera edad radiométrica de los depósitos Cretácicos de la Precordillera Central. Revista de la Asociación Geológica Argentina 62, 471–474.

Tobler, D.J., Stefánsson, A., Benning, L.G., 2008. In-situ grown silica sinters in Icelandic geothermal areas. Geobiology 6, 481–502.

Torsvik, T.H., Rousse, S., Labails, C., Smethurst, M.A., 2009. A new scheme for the opening of the South Atlantic Ocean and the dissection of an Aptian salt basin. Geophysical Journal International 177, 1315–1333.

Veysey, J., Fouke, B.W., Kandianis, M.T., Schickel, T.J., Johnson, R.W., Goldenfeld, N., 2008. Reconstruction of water temperature, ph, and flux of ancient hot springs from travertine depositional facies. Journal of Sedimentary Research 78, 69–76.

Webster, R.E., Chebli, G.A., Fischer, J.F., 2004. General Levalle Basin, Argentina: a frontier Lower Cretaceous rift basin. American Association of Petroleum Geologists, Bulletin 88, 627–652.

White, N.C., Hedenquist, J.W., 1990. Epithermal environments and styles of mineralization: variations and their causes, and guidelines for exploration. Journal of Geochemical Exploration 36, 445–474.

Wright, V.P., 1992. A revised classification of limestones. Sedimentary Geology 76, 177–185.

Yun, C.S., Yang, S.Y., 1997. Dinosaur eggshells from Hasandong Formation, Gyeongsang Supergroup, Korea. Journal of the Paleontological Society of Korea 13, 21–36.

Zhao, Z.K., 1979. Discovery of the dinosaurian eggs and footprint from Neixiang County, Henan Province. Vertebrata PalAsiatica 17, 304–309.

Zhao, Z.K., Ding, S.R., 1976. Discovery of the dinosaur eggs from Alashanzuoqi and its stratigraphical meaning. Vertebrata PalAsiatica 14, 42–44.

Zuzek, A.B., 1978. Descripción Geológica de la Hoja 18 f. Chamical, provincia de La Rioja. Boletín del Servicio Geológico Nacional, 161 pp.